

From Cs2Mo6Cl14 to Cs2Mo6Cl14×H2O and Vice Versa: Crystal Chemistry Investigations

N. Saito, P. Lemoine, N. Dumait, M. Amela-Cortes, Serge Paofai, T. Roisnel, V. Nassif, F. Grasset, Y. Wada, N. Ohashi, et al.

▶ **To cite this version:**

N. Saito, P. Lemoine, N. Dumait, M. Amela-Cortes, Serge Paofai, et al.. From Cs2Mo6Cl14 to Cs2Mo6Cl14×H2O and Vice Versa: Crystal Chemistry Investigations. Journal of Cluster Science, 2017, 28 (2), pp.773–798. 10.1007/s10876-016-1133-5 . hal-01515141

HAL Id: hal-01515141

https://univ-rennes.hal.science/hal-01515141

Submitted on 27 Oct 2020

HAL is a multi-disciplinary open access archive for the deposit and dissemination of scientific research documents, whether they are published or not. The documents may come from teaching and research institutions in France or abroad, or from public or private research centers.

L'archive ouverte pluridisciplinaire **HAL**, est destinée au dépôt et à la diffusion de documents scientifiques de niveau recherche, publiés ou non, émanant des établissements d'enseignement et de recherche français ou étrangers, des laboratoires publics ou privés.

From $Cs_2Mo_6Cl_{14}$ to $Cs_2Mo_6Cl_{14}.H_2O$ and vice versa: Crystal chemistry investigations

Norio Saito[1,2,3], Pierric Lemoine[4,a], Noée Dumait[4], Maria Amela-Cortes[4], Serge Paofai[4], Thierry Roisnel[4], Vivian Nassif[5], Fabien Grasset[2,6], Yoshiki Wada[2,3], Naoki Ohashi[2,3,7], Stéphane Cordier[4]

[1] Department of Metallurgy and Ceramics Science, Tokyo Institute of Technology (Tokyo Tech.), 2-12-1 Ookayama, Meguro, Tokyo 152-8551, Japan.
[2] Electroceramics Group, National Institute for Materials Science (NIMS), 1-1 Namiki, Tsukuba, Ibaraki 305-0044, Japan.
[3] NIMS-Saint-Gobain Center of Excellence for Advanced Materials, NIMS, 1-1 Namiki, Tsukuba, Ibaraki 305-0044, Japan.
[4] Institut des Sciences Chimiques de Rennes, UMR-CNRS 6226, 263 Avenue du Général Leclerc, CS 74205, 35042 Rennes Cedex, France.
[5] Institut Néel, CNRS/UGA UPR2940, 25 rue de Martyrs BP 166 38042 Grenoble Cedex 9, France.
[6] Laboratory for Innovative Key Materials and Structures (LINK, UMI 3629), NIMS, 1-1 Namiki, Tsukuba, Ibaraki 305-0044, Japan.
[7] Materials Research Center for Element Strategy (MCES), Tokyo Tech., Midori-ku, Yokohama 226-0026, Japan.

[a] corresponding authors: pierric.lemoine@univ-rennes1.fr, stephane.cordier@univ-rennes1.fr

From $Cs_2Mo_6Cl_{14}$ to $Cs_2Mo_6Cl_{14}.H_2O$ and vice versa: Crystal chemistry investigations

Abstract

We report here the synthesis, the crystal structure and the luminescent properties of the new cluster compounds $Cs_2Mo_6Cl_{14}.H_2O$ and $Cs_2Mo_6Br_{14}.H_2O$. Single-crystal X-ray diffraction performed on $Cs_2Mo_6Cl_{14}.H_2O$ indicates that the compound crystallizes in the monoclinic space group *C*2/*c* with refined cell parameters a = 19.578 Å, b = 15.151 Å, c = 9.347 Å, and β = 115.64°. The structure can be described from discrete $[Mo_6Cl^i_8Cl^a_6]^{2-}$ anionic cluster units arranged in a "A-A'-A-A'" pseudo prismatic stacking parallel to (*b*,*c*) plane with both Cs^+ cations and water molecules located between the layers. The centric character of the trigonal structure of $Cs_2Mo_6Cl_{14}$ was also studied by combination of single-crystal X-ray diffraction and both X-ray and neutron powder diffraction. The results suggest an important influence of the sample preparation on the symmetry of the crystal structure. The crystal structure relationship between the $[Mo_6Cl^i_8Cl^a_6]^{2-}$ anionic cluster unit arrangements in $Cs_2Mo_6Cl_{14}$ and $Cs_2Mo_6Cl_{14}.H_2O$ is discussed. Finally, the characterization of the luminescent properties of $Cs_2Mo_6X_{14}$ and $Cs_2Mo_6X_{14}.H_2O$ (X = Cl, Br) indicates that emission profile is comparable regardless existence of water molecule in the crystal structure.

Keywords: Metal atom clusters; Crystal structure; X-ray diffraction; Neutron diffraction; Luminescent materials

1. Introduction

Face-capped $Mo_6X^i_8X^a_6$ units containing octahedral molybdenum clusters are the basic buildings blocks of many inorganic solid state compounds, hybrid frameworks and nanomaterials [1-13]. Formation of Mo_6 cluster occurs at high temperatures via solid state reactions. Discrete anionic units $[Mo_6X^i_8X^a_6]^{2-}$ are found in inorganic solid state compounds when associated with divalent cations (*3d* metals, Pb^{2+}, Eu^{2+}…) or monovalent cations (alkaline metals) [14]. Among these compounds, $Cs_2Mo_6X^i_8X^a_6$ (X = Cl, Br and I) series is known for a long time and has been widely used as precursor for the preparation of hybrid nanomaterials due to their solubility in organic solvents like acetone, ethanol and acetonitrile [1,2,9,15], and unique photochemical features such as redox properties [16], photocatalysis [8,17,18], and photoluminescence [15]. For instance, with iodine, the substitution via solution chemistry of apical I^a by $OCOC_nF_{2n+1}$ groups leads to $Cs_2Mo_6I^i_8(OCOC_nF_{2n+1})^a_6$ (n = 1, 2, 3) series [19,20]. From the viewpoint of optical properties, the $[Mo_6I^i_8(OCOC_nF_{2n+1})^a_6]^{2-}$ units exhibit enhanced quantum yields compared to pure iodide $[Mo_6I^i_8I^a_6]^{2-}$. In the case of bromide, the interaction between $Cs_2Mo_6Br^i_8Br^a_6$ and crown ethers functionalized by promesogenic ligands in solution yields very interesting liquid crystal materials wherein Cs^+ cations are complexed with macrocycles [21,22]. Last but not least, the whole series $Cs_2Mo_6X^i_8X^a_6$ (X = Cl, Br and I) has been used as precursor for their integration in silica nanoparticles $Cs_2Mo_6X^i_8X^a_6@SiO_2$ [2,3,23-26].

Different routes to prepare $Cs_2Mo_6X^i_8X^a_6$ (X = Cl, Br and I) have been reported in literature: (i) solid state synthesis at high temperature from mixture of MoX_2 and CsX [14,27], (ii) synthesis from MoX_2 solution, AX salts and HX solution [28], and (iii) synthesis from derivative method reported by Flemström *et al.* [29] using $(H_3O)_2Mo_6X^i_8X^a_6.7H_2O$ solution [30] and AX salts. Preparation of highly pure $Cs_2Mo_6X^i_8X^a_6$ sample in high yield requires purification of the product by dissolution, filtration, and evaporation process. If it is soluble and stable in organic solvent, it turns out that $Cs_2Mo_6X^i_8X^a_6$ quickly react with water leading to exchanges of apical ligands (X^a) by hydroxo groups or water molecules. This precipitation is prevented by acidification of the water solution lower than pH = 2 or by addition of ethanol (50% Vol.). After dissolution in technical solvents (*i.e.* water containing solvents), it was pointed out that the crystal structure of $Cs_2Mo_6Cl_{14}$ can guest some water molecules without altering the cesium and cluster stacking [31]. Addition of large amount of water molecules in the Cs^+ and $[Mo_6Cl^i_8Cl^a_6]^{2-}$ frameworks leads to crystal structure modification with the formation of $Cs_2Mo_6Cl^i_8Cl^a_6.3H_2O$ wherein water molecules interact with cluster units through hydrogen bonding to form its crystalline frameworks [29].

This work focuses on the structural characterization of a new monohydrated cluster compound $Cs_2Mo_6Cl^i_8Cl^a_6.H_2O$ using single-crystal and powder diffraction, and the measurement of its luminescent properties. It is evidenced that the water molecule of $Cs_2Mo_6Cl^i_8Cl^a_6.H_2O$ is easily de-intercalated and then the crystal structure transforms to $Cs_2Mo_6Cl^i_8Cl^a_6$. Last but not least, the centric character of the trigonal crystal

structure of $Cs_2Mo_6Cl^i_8Cl^a_6$ is also discussed on the basis of single crystal and powder diffraction studies using X-ray and neutron radiations.

2. Experimental methods

2.1. Synthesis

The synthesis of $Cs_2Mo_6Cl_{14}$ powder was performed according to a derivative method from that reported by Healy *et al.* [32]. In a first step, $(H_3O)_2Mo_6Cl_{14}.7H_2O$ was prepared as single crystals using method reported by Koknat *et al.* [30]. In a second step 10 g of $(H_3O)_2Mo_6Cl_{14}.7H_2O$ (8.1 mmol) and 2.75 g of CsCl (16.3 mmol) were dissolved separately in 10 ml of ethanol and heated until ebullition. Then, the solution of CsCl was added to the cluster solution under stirring. After evaporation of solvent to dryness, $Cs_2Mo_6Cl_{14}$ and $Cs_2Mo_6Cl_{14}.H_2O$ were extracted from the remaining solid by dissolution in acetone and the powders were crystallized from the filtrate by solvent evaporation with a rotavapor at 60°C and room temperature, respectively. The resulting powders were stored under air at room temperature.

2.2. Single-crystal X-ray diffraction

Table 1: Summary of single crystal data collections and structure refinement conditions at room temperature and 150 K of $Cs_2Mo_6Cl_{14}$

Structural formula	$Cs_2Mo_6Cl_{14}$	$Cs_2Mo_6Cl_{14}$	$Cs_2Mo_6Cl_{14}$	$Cs_2Mo_6Cl_{14}$
Space group	*P*-31*c*	*P*31*c*	*P*-31*c*	*P*31*c*
Temperature (K)	293(2)	293(2)	150(2)	150(2)
Formula weight	1337.76	1337.76	1337.76	1337.76
Wavelength (Å)	0.71073	0.71073	0.71073	0.71073
Crystal system	Trigonal	Trigonal	Trigonal	Trigonal
a (Å)	9.8225(11)	9.8225(11)	9.7786(4)	9.7786(4)
b (Å)	9.8225(11)	9.8225(11)	9.7786(4)	9.7786(4)
c (Å)	14.1967(18)	14.1967(18)	14.0895(7)	14.0895(7)
V ($Å^3$)	1186.2(3)	1186.2(3)	1166.8(2)	1166.8(2)
Z	2	2	2	2
Calculated density ($g.cm^{-3}$)	3.745	3.745	3.808	3.808
Absorption coefficient (mm^{-1})	7.663	7.663	7.791	7.791
F(000)	1200	1200	1200	1200
Crystal size (mm)	0.10 × 0.04 × 0.035	0.10 × 0.04 × 0.035	0.10 × 0.04 × 0.035	0.10 × 0.04 × 0.035
Crystal color	Yellow	Yellow	Yellow	Yellow
Theta range (°)	3.739 - 33.113	3.739 - 33.113	3.762 - 33.116	3.762 - 33.116
h_min, h_max	-15, 14	-15, 14	-15, 13	-15, 13
k_min, k_max	-13, 15	-13, 15	-10, 15	-10, 15
l_min, l_max	-15, 21	-15, 21	-14, 21	-14, 21
R(int)	0.0894	0.0667	0.0706	0.0368
Reflections collected	9931	9931	8929	8929
Reflections unique [I>2σ]	1142	1955	1272	2124
Completeness	0.997	0.997	0.997	0.997
Data/restraints/ parameters	1512/0/36	2657/1/67	1490/0/36	2553/1/67
Flack parameter	-	0.64(9)	-	0.53(7)
Goodness-of-fit	1.261	1.039	1.283	1.089
Final R_1 [I>2σ]	0.0906	0.0623	0.1274	0.0571
Final wR_2 [I>2σ]	0.1978	0.1449	0.2858	0.1427
Largest difference ($e.Å^{-3}$)	3.824 and -3.074	3.020 and -2.501	4.525 and -5.170	4.978 and -3.174

Single crystals of $Cs_2Mo_6Cl_{14}$ and $Cs_2Mo_6Cl_{14}.H_2O$ were obtained from the aforementioned precursor by slow evaporation of an acetonitrile solution with dichloromethane as antisolvent, both stored under ambient atmosphere. The crystal structure measurements have been performed on D8 Venture Bruker AXS diffractometer for $Cs_2Mo_6Cl_{14}$ and on APEX II Bruker AXS diffractometer for $Cs_2Mo_6Cl_{14}.H_2O$, using both Mo-K_α X-ray wavelength (λ = 0.71073 Å) at the Centre de Diffractométrie X de l'Institut des Sciences Chimiques de Rennes. Measurements were carried out at room temperature (T = 293K) and low temperature (T = 150K) in

order to check any influence of the temperature on the crystallographic structures. The structures were solved by direct methods using the SIR97 program [33], and then refined with full-matrix least-square methods based on F^2 (SHELXL-2014) [34] using the WinGX software package [35]. All non-hydrogen atoms were refined with anisotropic atomic displacement parameters. Hydrogen atom was introduced in the structural model through Fourier difference maps analysis. Hydrogen atomic coordinates were refined, while the equivalent isotropic displacement parameter was constrained to be equal to 1.2 times that of the oxygen atom. The conditions of data collection and structure refinements are gathered in Table 1 for $Cs_2Mo_6Cl_{14}$ and in Table 2 for $Cs_2Mo_6Cl_{14}.H_2O$. Further details of the crystal structure investigations may be obtained from FIZ Karlsruhe, 76344 Eggenstein-Leopoldshafen, Germany (fax: (+49)7247-808-666; e-mail: crysdata@fiz-karlsruhe.de, on quoting the deposition numbers CSD-431922, -431923, -431924, -431925, -431926, and -431927.

Table 2: Summary of single crystal data collections and structure refinement conditions at room temperature and 150 K of $Cs_2Mo_6Cl_{14}.H_2O$

Structural formula	$Cs_2Mo_6Cl_{14}.H_2O$	$Cs_2Mo_6Cl_{14}.H_2O$
Space group	*C*2/*c*	*C*2/*c*
Temperature (K)	293(2)	150(2)
Formula weight	1355.78	1355.78
Wavelength (Å)	0.71073	0.71073
Crystal system	Monoclinic	Monoclinic
a (Å)	19.5638(8)	19.5004(11)
b (Å)	15.1414(6)	15.1808(8)
c (Å)	9.3402(4)	9.3527(5)
β (°)	115.632(2)	115.698(3)
V (Å^3)	2494.5(2)	2494.8(2)
Z	4	4
Calculated density (g.cm^{-3})	3.610	3.610
Absorption coefficient (mm^{-1})	7.294	7.293
F(000)	2440	2440
Crystal size (mm)	0.15 × 0.09 × 0.05	0.15 × 0.09 × 0.05
Crystal color	Yellow	Yellow
Theta range (°)	3.379 - 41.253	3.379 - 40.881
h_min, h_max	-35, 36	-30, 35
k_min, k_max	-28, 28	-27, 27
l_min, l_max	-17, 17	-17, 17
R(int)	0.0535	0.0402
Reflections collected	29227	32872
Reflections unique [I>2σ]	5023	6239
Completeness	0.989	0.993
Data/restraints/ parameters	8265/0/110	8112/0/110
Goodness-of-fit	0.996	1.017
Final R_1 [I>2σ]	0.0370	0.0279
Final wR_2 [I>2σ]	0.0651	0.0455
Largest difference (e.Å^{-3})	1.167 and -2.055	1.046 and -1.541

2.3. X-ray and neutron powder diffraction

X-ray powder diffraction (XRPD) data were collected at room temperature using a Bruker D8 Advance two-circle diffractometer (θ-2θ Bragg-Brentano mode) using Cu K_α radiation (λ = 1.54056 Å) equipped with a Ge(111) monochromator and a Lynx Eye detector. Neutron powder diffraction (NPD) experiments were carried out at the Institut Laue Langevin (ILL), Grenoble, France. The data were collected at room temperature using the high-resolution neutron two-axis powder diffractometer D1b (λ = 2.52 Å) equipped with a one-dimensional curved multidetector. The analysis of the diffraction patterns was performed by Rietveld profile refinement using the FullProf and WinPlotr software packages [36,37]. These softwares were also used to performed XRPD simulations from single-crystal refinements.

2.4. Photoluminescence measurement

The photoluminescence studies were performed using 820 nm output of a Coherent Mira 900-F mode-locked Ti:Sapphire (Ti-Sap) laser pumped by a Verdi 5 W, with 130 fs pulse width, and 76MHz repetition rate. The

light pulse was sent through a Coherent 5-050 SHG generator to generate 410 nm light as the excitation source. The luminescence of the sample was passed through an Acton Research VM-505 monochromator and detected by an InGaAs photodiode.

3. Crystallographic results

3.1. Single-crystal X-ray diffraction of $Cs_2Mo_6Cl_{14}$

As earlier reported in the publication of Healy *et al.* [32], the systematic extinctions observed on the crystal data of $Cs_2Mo_6Cl_{14}$ allow structural refinements in two possible space groups: *P*31*c* (space group No.159) or *P*-31*c* (space group No.163). In the centrosymmetric space group *P*-31*c*, all crystallographic sites are fully occupied by the respective atoms except one of the two Cs cationic sites. Cs atoms are located on two Wyckoff positions: Cs1 on *4e* (0, 0, z) with a 50% occupancy factor and Cs2 on *2c* (1/3, 2/3, 1/4). Mo atoms are located on position *12i* (x, y, z), and Cl atoms are located on one position *4f* (1/3, 2/3, z) and two positions *12i* (x, y, z) (Table 3 and Table 4). In the non-centrosymmetric space group *P*31*c*, all crystallographic sites are fully occupied, including Cs1 site. Cs atoms are located on two Wyckoff positions: Cs1 on *2a* (0, 0, z) and Cs2 on *2b* (1/3, 2/3, z). Mo atoms are located on two positions *6c* (x, y, z), and Cl atoms are located on two positions *2b* (1/3, 2/3, z) and four positions *6c* (x, y, z) (Table 3 and Table 4).

Table 3: Atomic coordinates, site occupancy and equivalent isotropic displacement parameters of $Cs_2Mo_6Cl_{14}$ refined at room temperature

P-31*c*						
Atom	Site	x	y	z	Occ.	U(eq)
Cs1	4e	0	0	0.0203(5)	0.50	0.046(2)
Cs2	2c	1/3	2/3	0.2500	1.00	0.0516(9)
Mo1	12i	0.5138(2)	0.3350(2)	0.1751(1)	1.00	0.0139(2)
Cl1	4f	2/3	1/3	0.0390(3)	1.00	0.0210(10)
Cl2	12i	0.3752(4)	0.0452(4)	0.1770(2)	1.00	0.0239(6)
Cl3	12i	0.3085(4)	0.3467(5)	0.0855(3)	1.00	0.0334(8)

*P*31*c*						
Atom	Site	x	y	z	Occ.	U(eq)
Cs1	2a	0	0	0.0262(3)	1.00	0.0500(7)
Cs2	2b	1/3	2/3	0.2514(4)	1.00	0.0510(6)
Mo1a	6c	0.5158(2)	0.3383(2)	0.1798(1)	1.00	0.0132(3)
Mo1b	6c	0.5113(2)	0.1809(2)	0.3293(1)	1.00	0.0140(3)
Cl1a	2b	2/3	1/3	0.0417(6)	1.00	0.0195(18)
Cl1b	2b	2/3	1/3	0.4653(6)	1.00	0.0224(19)
Cl2a	6c	0.3706(5)	0.0479(5)	0.1823(3)	1.00	0.0206(9)
Cl2b	6c	0.3788(5)	0.3382(5)	0.3276(4)	1.00	0.0209(9)
Cl3a	6c	0.3140(7)	0.3549(7)	0.0891(4)	1.00	0.0294(11)
Cl3b	6c	0.6620(7)	0.6959(7)	0.4183(4)	1.00	0.0351(13)

The lowest values of R(int) = $\sum|F_o^2 - \langle F_o^2\rangle|/\sum[F_o^2]$, related to the number of unique reflections measured, for *P*31*c* compared to *P*-31*c* should favors the non-centrosymmetric space group (Table 1). However, the crystal structure can be equally well refined either in *P*-31*c* or *P*31*c* space group. The best reliability factors (goodness-of-fit, final R_1 and final wR_2 factors) along with lowest electron density differences are obtained for refinements performed using space group *P*31*c* (Table 1). Considering that both resulting structural models are physically meaningful, these apparent improvements can be simply related to a large number of free parameters allowed by the space group *P*31*c* compared to the space group *P*-31*c* (Table 1). So, it is necessary to go deeper in the interpretation of results.

The refinement in *P*31*c* space group instead of *P*-31*c* induces to double positions of Mo and Cl atoms owing to the loss of inversion center (Figure 1, Table 3 and Table 4), allowing independent rotations of the two $[Mo_6Cl^i{}_8Cl^a{}_6]^{2-}$ units around three fold axis of the unit cell. A noticeable difference concerns the position of cesium cations. In *P*-31*c*, Cs1 half occupies a *4e* position with a 3 site symmetry (C_3 according to Schoenflies notation) whereas it fully occupies a *2a* position with a 3 site symmetry (C_3 according to Schoenflies notation) in *P*31*c*. In *P*-31*c*, Cs2 fully occupies a *2c* position with a 32 site symmetry (D_3 according to Schoenflies notation)

and it fully occupies a *2b* position with a 3 site symmetry (C_3 according to Schoenflies notation) in *P*31*c* (Figure 2). The change of site symmetry position for Cs2 from *P*-31*c* to *P*31*c* implies the refinement of *z* coordinate in the latter space group (Table 3 and Table 4). Thus, the loss of the symmetry center in *P*31*c* induces independent rotations of the cluster units and the possibility of motion of Cs2 along 3 fold axis, which may explain the improvement of reliability factors for the *P*31*c* space group compared to *P*-31*c*. In order to be confident in non-centro symmetric model, additional possible symmetry and in particular correlation of Mo and Cl positions in the two independent units through inversion center were envisioned. Hence, the model was checked with Addsym program [38,39] and no obvious additional symmetry as inversion center could be detected. However, the values of the Flack parameter (0.64(9) at room temperature and 0.53(7) at 150 K, Table 1) suggest that the model in *P*31*c* is very close to centro-symmetry.

Table 4: Atomic coordinates, site occupancy and equivalent isotropic displacement parameters of $Cs_2Mo_6Cl_{14}$ refined at 150 K

P-31*c*						
Atom	Site	x	y	z	Occ.	U(eq)
Cs1	4e	0	0	0.0317(5)	0.50	0.031(2)
Cs2	2c	1/3	2/3	0.2500	1.00	0.0280(8)
Mo1	12i	0.5136(2)	0.3356(2)	0.1747(2)	1.00	0.0084(3)
Cl1	4f	2/3	1/3	0.0379(5)	1.00	0.0117(12)
Cl2	12i	0.3733(6)	0.0450(6)	0.1761(3)	1.00	0.0159(9)
Cl3	12i	0.3069(6)	0.3479(8)	0.0842(4)	1.00	0.0212(10)

*P*31*c*						
Atom	Site	x	y	z	Occ.	U(eq)
Cs1	2a	0	0	0.0366(2)	1.00	0.0293(4)
Cs2	2b	1/3	2/3	0.2488(2)	1.00	0.0283(4)
Mo1a	6c	0.5161(2)	0.3402(2)	0.1790(1)	1.00	0.0082(3)
Mo1b	6c	0.5100(2)	0.1813(2)	0.3294(1)	1.00	0.0078(3)
Cl1a	2b	2/3	1/3	0.0401(5)	1.00	0.0114(12)
Cl1b	2b	2/3	1/3	0.4664(5)	1.00	0.0114(11)
Cl2a	6c	0.3684(4)	0.0483(4)	0.1811(3)	1.00	0.0122(7)
Cl2b	6c	0.3789(4)	0.3410(4)	0.3275(3)	1.00	0.0119(6)
Cl3a	6c	0.3156(4)	0.3599(5)	0.0873(3)	1.00	0.0167(7)
Cl3b	6c	0.6678(5)	0.7013(5)	0.4186(3)	1.00	0.0193(8)

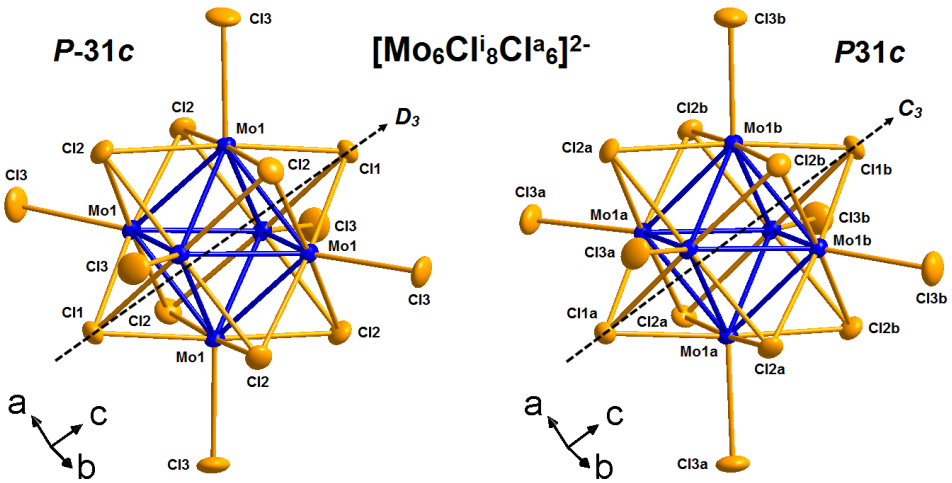


Figure 1: Representation of the discrete $[Mo_6Cl^i_8Cl^a_6]^{2-}$ anionic cluster unit at room temperature in $Cs_2Mo_6Cl_{14}$ refined in the centrosymmetric space group *P*-31*c* (left) and refined in the non-centrosymmetric space group *P*31*c* (right). Displacement ellipsoids are shown at the 50 % probability level

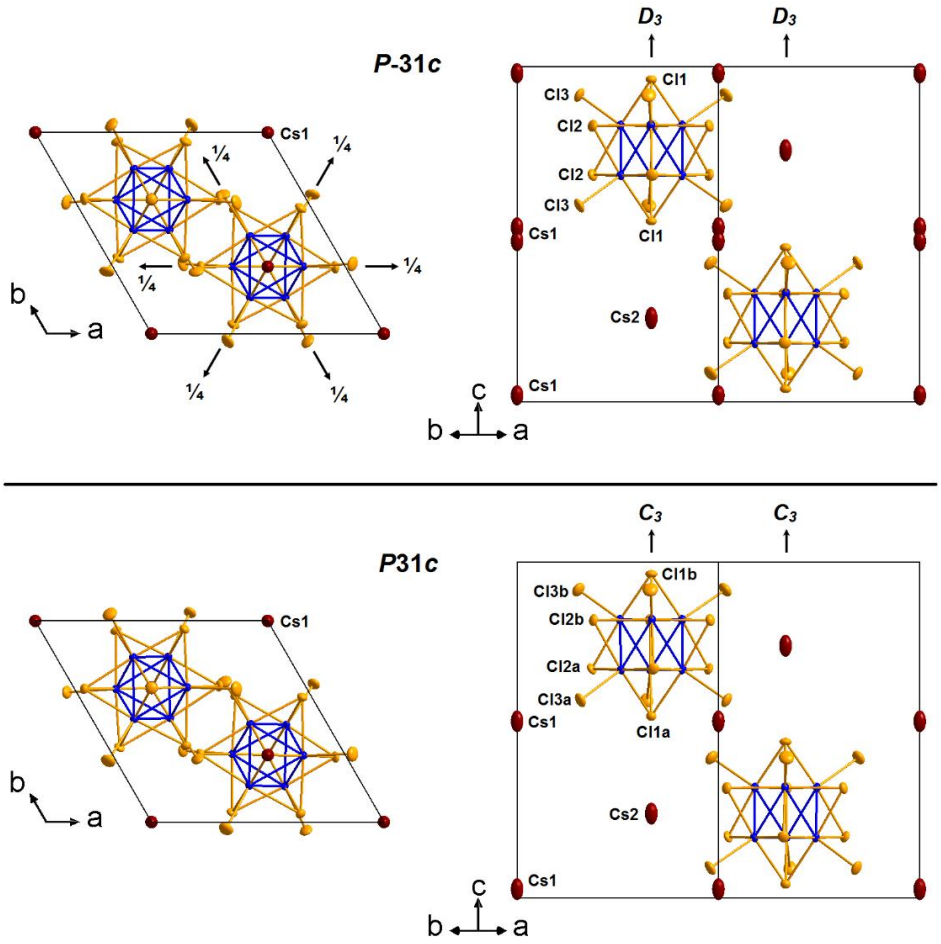


Figure 2: Representations of the $Cs_2Mo_6Cl_{14}$ unit cell at room temperature refined in the centrosymmetric space group *P*-31*c* (up) and refined in the non-centrosymmetric space group *P*31*c* (bottom). Displacement ellipsoids are shown at the 50 % probability level

Regardless the space group, the crystal structure of $Cs_2Mo_6Cl_{14}$ consists of two $[Mo_6Cl_{14}]^{2-}$ units per unit cell located on the crystallographic three-fold axes and related by the (1-10) glide plane (Figure 2). Cs^+ cations occupy special positions on the three-fold axes. This structure can be described using approach used for $Cs_2Mo_6Br_{14}$ [27]. Discrete $[Mo_6Cl^i_8Cl^a_6]^{2-}$ anionic cluster units are arranged in a "A-B-A-B" close-packed hexagonal stacking along the *c*-axis with three-fold axes of the clusters perpendicular to the hexagonal planes. Cs^+ cations are located either in the octahedral sites (Cs1) or in one half of the triangular sites (Cs2) formed by the cluster framework (Figure 3).

Refinements performed at 293 K and 150 K lead to similar refined atomic coordinates (Table 3 and Table 4) indicating no structural modification on this temperature range. However, in relation with the reduction of the atomic thermal motion, both isotropic (Table 3 and Table 4) and anisotropic (Table S1 and Table S2) displacement parameters are lower at 150 K compared to those refined at 293 K. Finally, non-negligible residual positive electron difference of ≈ 3 $e^-.Å^{-3}$ at room temperature and ≈ 5 $e^-.Å^{-3}$ at 150 K have been detected at the position (0, 0, ≈0.25) (Table 1), *i.e.* unoccupied triangular site, which can be a consequence of either weak Cs disorder or water/solvent molecule insertion. While the former possibility is not excluded, the latter appears more realistic considering the preparation route used.

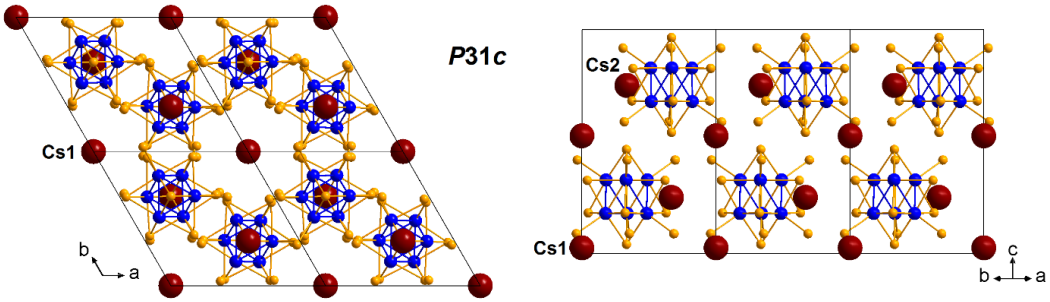


Figure 3: Crystal structure representations of $Cs_2Mo_6Cl_{14}$ considering the non-centrosymmetric space group *P*31*c*

Within the cluster units, the molybdenum octahedral clusters are face-capped by eight chlorine atoms (*i.e.* Cl1 and Cl2), the six others chlorine atoms (*i.e.* Cl3) being located in apical positions (Figure 1). It could be observed higher atomic displacement parameters for chlorines in apical positions compared to chlorines in inner positions (Table 3, Table 4, Table S1, and Table S2). This feature is explained by the fact that apical ligands are bonded only to one molybdenum atom compared to three molybdenum for inner ones. The shortest Mo-Cl bond distances in $[Mo_6Cl^i_8Cl^a_6]^{2-}$ units are encountered between Mo atoms and Cl atoms in apical positions (Table 5). This is the reverse situation for larger ligands X like Br and I owing to steric hindrance of inner ligands (*i.e.* $d(Mo\text{-}X^i) < d(Mo\text{-}X^a)$).

Table 5: Average bond distances in $[Mo_6Cl^i_8Cl^a_6]^{2-}$ units

Compound	Space group	Mo-Mo (Å)	Mo-Cl^i (Å)	Mo-Cl^a (Å)	Δ^1
T = 293 K					
$Cs_2Mo_6Cl_{14}$	*P*-31*c*	2.611	2.470	2.436	+1.40
$Cs_2Mo_6Cl_{14}.H_2O$	*C*2/*c*	2.605	2.473	2.437	+1.48
T = 150 K					
$Cs_2Mo_6Cl_{14}$	*P*-31*c*	2.608	2.467	2.443	+0.98
$Cs_2Mo_6Cl_{14}.H_2O$	*C*2/*c*	2.620	2.486	2.450	+1.47

$^1\Delta = (Mo\text{-}Cl^i - Mo\text{-}Cl^a)/Mo\text{-}Cl^a$ (%)

In conclusion, the difficulty to determine accurately by single-crystal X-ray diffraction technique if the crystal structure of $Cs_2Mo_6Cl_{14}$ is centric or not is related to (i) the higher disorder of cesium atoms in comparison to the $[Mo_6Cl^i_8Cl^a_6]^{2-}$ cluster unit framework, as suggested by both the isotropic (Table 3 and Table 4) and anisotropic (Table S1 and Table S2) displacement parameters of the corresponding atoms and (ii) the difficulty to conclude unambiguously to the punctual presence of water/solvent molecules in the unoccupied triangular site. According to Marsh [40], if a centrosymmetric description, even one that involves disorder, provides adequate agreement between observed and calculated intensity, there is no profit in searching further. If small deviations from centrosymmetry are present, they must be detected by others means.

3.2. X-ray and neutron powder diffraction of $Cs_2Mo_6Cl_{14}$ and $Cs_2Mo_6Br_{14}$

X-ray powder diffraction patterns (λ = 1.54056 Å) simulated from both the *P*-31*c* and *P*31*c* single-crystal X-ray models of $Cs_2Mo_6Cl_{14}$ are shown in Figure 4. These XRPD simulations are very similar, except for some very weak intensity diffraction peaks (*i.e.* (3 0 1) and (3 0 3) reflections) which appear to have an intensity close to zero with the centrosymmetric structure, and are clearly observed in logarithmic intensity scale with the non-centrosymmetric structure (insets of Figure 4), due to a weak change in their structure factors.

$Cs_2Mo_6Cl_{14}$ sample has been analyzed by combined Rietveld refinement of neutron and X-ray powder diffraction data (Figure 5). In contrary to the single-crystal sample freshly prepared by solvent evaporation, the powder sample was well dried before analyses. A better accuracy on the refined cell parameters is obtained from X-ray diffraction data than those of neutron, due to shorter wavelength and thinner diffraction peaks in X-ray diffraction measurement. That could explain the non-negligible differences observed in the refined cell parameters between neutron and X-ray data (Table 6). However, taking into account more close values of the neutron scattering lengths [41] of Cs (5.42 fm), Mo (6.715 fm), and Cl (9.577 fm) compared to their respective atomic number Z, neutron diffraction data is more suitable to probe accurate atomic coordinates in the refinement. Moreover, considering the neutron scattering lengths of oxygen (5.803 fm) and hydrogen (-3.739 fm) for one hand, and the large incoherent scattering length of H atoms for the other hand, presence of solvent

molecules in the sample should be detected by neutron diffraction. Considering the signal to noise ratio of the neutron data and the quality of the refinement (Figure 5 and Table 7), presence of solvent molecules in the powder sample can be excluded. The refined atomic coordinates and Debye-Waller factors, gathered in Table 7, are in excellent agreement with results obtained from single-crystal X-ray data (Table 3). The absence of the (3 0 1) and (3 0 3) diffractions peaks on both X-ray and neutron powder diffraction data (Figure 5) suggests that dry $Cs_2Mo_6Cl_{14}$ powder crystallizes in the centrosymmetric space group *P*-31*c*. In addition, similar conclusion can be also deduced from combined Rietveld refinement with X-ray and neutron powder diffraction data of the $Cs_2Mo_6Br_{14}$ powder sample (Figure S1). The refined structural parameters at room temperature of $Cs_2Mo_6Br_{14}$ are gathered in Table 6 and Table 7. These results are in fair agreement with recent optical results reported on $Cs_2Mo_6Cl_{14}$ powder after heat treatment where the absence of second harmonic generation (SHG) signal indicates that $Cs_2Mo_6Cl_{14}$ exhibits an inversion symmetry [31].

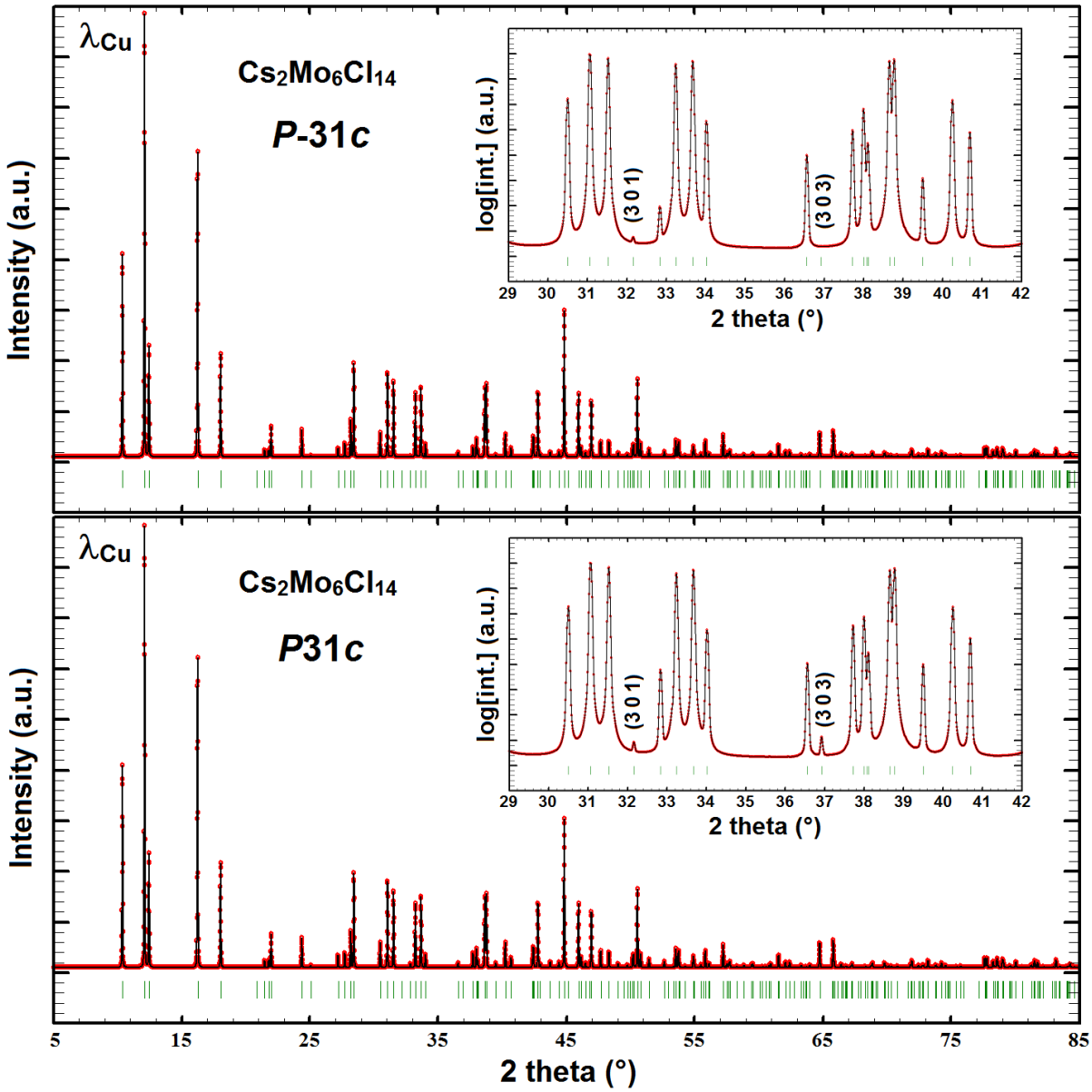


Figure 4: XRPD pattern simulations of $Cs_2Mo_6Cl_{14}$ considering models obtained by structural refinements using either centrosymmetric space group *P*-31*c* (top pattern) or non-centrosymmetric space group *P*31*c* (bottom pattern)

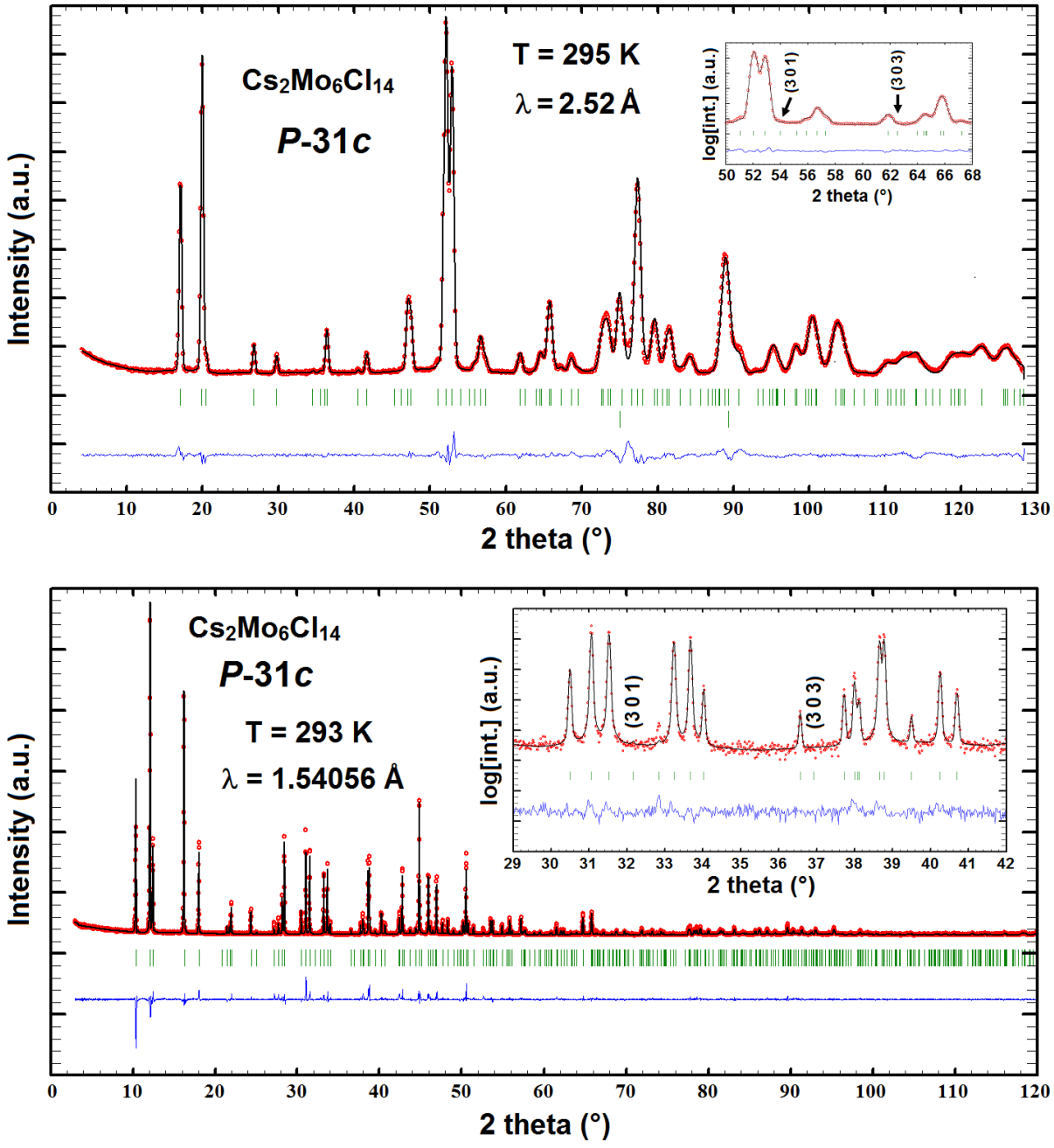


Figure 5: Combined neutron (top pattern) and X-ray (bottom pattern) powder diffraction refinement of $Cs_2Mo_6Cl_{14}$ at room temperature with centrosymmetric space group *P*-31*c*

Table 6: Cell parameters of $Cs_2Mo_6Cl_{14}$ and $Cs_2Mo_6Br_{14}$ at room temperature and reliability factors from combined neutron (λ = 2.52 Å) and X-ray (λ = 1.54056 Å) powder diffraction refinement (space group *P*-31*c*)

	$Cs_2Mo_6Cl_{14}$		$Cs_2Mo_6Br_{14}$	
P-31*c*	Neutron	X-ray	Neutron	X-ray
a (Å)	9.805(1)	9.821(1)	10.156(1)	10.196(2)
c (Å)	14.170(2)	14.195(2)	15.027(2)	15.086(4)
V (Å^3)	1179.6(2)	1185.8(2)	1342.4(2)	1358.2(5)
R_{Bragg} ; R_f	2.70 ; 2.30	11.4 ; 11.6	1.36 ; 1.05	9.29 ; 6.63
R_{wp} ; R_{exp}	2.19 ; 0.22	14.6 ; 7.28	1.53 ; 0.21	12.7 ; 7.22
χ^2	103	4.02	52.9	3.09

Table 7: Room temperature atomic coordinates, site occupancy and equivalent isotropic displacement parameters of $Cs_2Mo_6Cl_{14}$ and $Cs_2Mo_6Br_{14}$ refined in *P*-31*c* from combined neutron (λ = 2.52 Å) and X-ray (λ = 1.54056 Å) powder diffraction data

$Cs_2Mo_6Cl_{14}$						
Atom	Site	x	y	z	Occ.	B_{iso}
Cs1	4e	0	0	0.028(2)	0.50	2.5(4)
Cs2	2c	1/3	2/3	0.250	1.00	2.5(4)
Mo1	12i	0.514(1)	0.337(1)	0.175(1)	1.00	1.5(2)
Cl1	4f	2/3	1/3	0.039(1)	1.00	1.6(2)
Cl2	12i	0.374(1)	0.044(1)	0.178(1)	1.00	1.6(2)
Cl3	12i	0.310(1)	0.345(1)	0.085(1)	1.00	2.9(2)
$Cs_2Mo_6Br_{14}$						
Atom	Site	x	y	z	Occ.	B_{iso}
Cs1	4e	0	0	0.018(3)	0.50	2.0(4)
Cs2	2c	1/3	2/3	0.250	1.00	2.0(4)
Mo1	12i	0.516(1)	0.332(1)	0.179(1)	1.00	1.2(1)
Br1	4f	2/3	1/3	0.041(1)	1.00	1.1(2)
Br2	12i	0.367(1)	0.041(1)	0.179(1)	1.00	1.1(2)
Br3	12i	0.309(1)	0.344(1)	0.086(1)	1.00	2.3(2)

3.3. Single-crystal X-ray diffraction of $Cs_2Mo_6Cl_{14}.H_2O$

A new monoclinic compound containing $[Mo_6Cl^i_8Cl^a_6]^{2-}$ clusters has been stabilized by slow evaporation of an acetonitrile solution of $Cs_2Mo_6Cl_{14}$ with dichloromethane as antisolvent. Single-crystal XRD measurement has been performed at room temperature and at 150 K. Summary of data collections and structure refinement conditions are gathered in Table 2. This new compound crystallizes in the monoclinic *C*2/*c* space group (No.15) with refined cell parameters *a* = 19.5638(8) Å, *b* = 15.1414(6) Å, *c* = 9.3402(4) Å, β = 115.632(2)°, and V = 2494.5(2) $Å^3$ at room temperature (Table 2). The same space group and similar cell parameters have been already reported for $Rb_2Mo_6Cl_{14}$ [14], $Rb_2W_6Br_{14}$ [42], and $Rb_2Mo_6Br_{14}$ [43]. $(NH_4)_2Mo_6Cl_{14}.H_2O$ has been reported as the *I*2/*a* space group (No.15) description [44]. Flemström *et al.*, has also reported crystal structures of some monohydrated metal-cluster compounds, *i.e.* $(NH_4)_2Mo_6Cl_{14}.H_2O$, $K_2Mo_6Cl_{14}.H_2O$, and $Rb_2Mo_6Cl_{14}.H_2O$ [29]. However, in those compounds the lower symmetry space group *Ia* (*i.e.* Cc, No.9) has been rather suitable to account for slight disorder [29] instead of the space group *I*2/*a* (*i.e. C*2/c, No.15).

The structural refinement performed here indicates that Cs atoms are located on two Wyckoff positions: Cs1 on *4a* (0, 0, 0) and Cs2 on *4e* (0, y, 1/4). Mo atoms are located on three positions *8f* (x, y, z), and Cl atoms are located on seven position *8f* (x, y, z) (Table 8). All sites are fully occupied by the respective atoms. Positive residual electron difference detected on a *4e* (0, ≈0.155, ¼) position (*i.e.* triangular site formed by $[Mo_6Cl_{14}]^{2-}$ units) suggests either Cs disorder or solvent insertion into the crystal structure. Further refinement indicates a full occupation of the cesium sites, and then the positive residual electron difference can be perfectly accounted assuming insertion of one oxygen atom from water molecule on the *4e* (0, ≈0.155, ¼) site. These results allow us to conclude that the new compound crystallizing in monoclinic symmetry is $Cs_2Mo_6Cl_{14}.H_2O$. Hydrogen atoms were introduced in the structural model through Fourier difference maps analysis. Their atomic coordinates were refined but their equivalent isotropic displacement parameter was constrained to be equal to 1.2 times that of the oxygen atom. With this model, the largest absolute residual electron difference is ≤ 2 $e^-.Å^{-3}$ (Table 2), suggesting that no more atoms were missed. It is worth noting that addition of some drops of water in the acetonitrile solution really favors crystallization of this compound, supporting the existence of water in the monoclinic crystal structure. Moreover, the extra diffraction peaks observed on the diffraction pattern of the freshly prepared $Cs_2Mo_6Cl_{14}$ sample reported by Saito *et al.*, [31] fit perfectly with the pattern simulation of this hydrate cluster compound. To the best of our knowledge, this compound was never yet reported in literature.

Table 8: Atomic coordinates, site occupancy and equivalent isotropic displacement parameters refined at room temperature and 150 K for $Cs_2Mo_6Cl_{14}.H_2O$

T = 293 K						
Atom	Site	x	y	z	Occ.	U(eq)
Cs1	4a	0	0	0	1.00	0.0534(2)
Cs2	4e	0	0.4416(1)	¼	1.00	0.0351(1)
Mo1	8f	0.2067(1)	0.2700(1)	0.1380(1)	1.00	0.0191(1)
Mo2	8f	0.2964(1)	0.3584(1)	0.0503(1)	1.00	0.0190(1)
Mo3	8f	0.3328(1)	0.1992(1)	0.1625(1)	1.00	0.0188(1)
Cl1	8f	0.3317(1)	0.3235(1)	0.3322(1)	1.00	0.0266(2)
Cl2	8f	0.1746(1)	0.4208(1)	0.0250(1)	1.00	0.0259(2)
Cl3	8f	0.4141(1)	0.2864(1)	0.0719(1)	1.00	0.0258(2)
Cl4	8f	0.2440(1)	0.1184(1)	0.2368(1)	1.00	0.0267(2)
Cl5	8f	0.1479(1)	0.2961(1)	0.3170(2)	1.00	0.0390(2)
Cl6	8f	0.3590(1)	0.5015(1)	0.1164(2)	1.00	0.0332(2)
Cl7	8f	0.4422(1)	0.1304(1)	0.3768(2)	1.00	0.0347(2)
O1	4e	0	0.1550(4)	¼	1.00	0.092(2)
H1	8f	0.032(4)	0.187(4)	0.272(9)	1.00	0.110

T = 150 K						
Atom	Site	x	y	z	Occ.	U(eq)
Cs1	4a	0	0	0	1.00	0.0234(1)
Cs2	4e	0	0.4418(1)	¼	1.00	0.0170(1)
Mo1	8f	0.2066(1)	0.2691(1)	0.1396(1)	1.00	0.0092(1)
Mo2	8f	0.2957(1)	0.3593(1)	0.0496(1)	1.00	0.0092(1)
Mo3	8f	0.3344(1)	0.2001(1)	0.1632(1)	1.00	0.0091(1)
Cl1	8f	0.3326(1)	0.3244(1)	0.3334(1)	1.00	0.0131(1)
Cl2	8f	0.1725(1)	0.4201(1)	0.0252(1)	1.00	0.0128(1)
Cl3	8f	0.4147(1)	0.2890(1)	0.0703(1)	1.00	0.0126(1)
Cl4	8f	0.2462(1)	0.1177(1)	0.2392(1)	1.00	0.0131(1)
Cl5	8f	0.1476(1)	0.2944(1)	0.3201(1)	1.00	0.0186(2)
Cl6	8f	0.3574(1)	0.5034(1)	0.1150(1)	1.00	0.0159(1)
Cl7	8f	0.4453(1)	0.1319(1)	0.3786(1)	1.00	0.0166(1)
O1	4e	0	0.1525(2)	¼	1.00	0.040(1)
H1	8f	0.031(2)	0.186(2)	0.273(5)	1.00	0.048

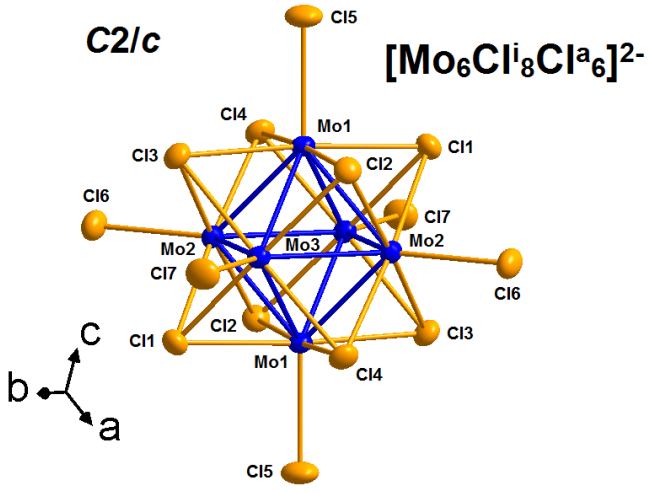


Figure 6: Representation of the discrete $[Mo_6Cl^i_8Cl^a_6]^{2-}$ anionic cluster unit at room temperature in $Cs_2Mo_6Cl_{14}.H_2O$. Displacement ellipsoids are shown at the 50 % probability level

Within the cluster units, the molybdenum octahedral clusters are face-capped by eight chlorine atoms (*i.e.* Cl1, Cl2, Cl3, and Cl4), the six others chlorine atoms (*i.e.* Cl5, Cl6, and Cl7) being located in apical positions (Figure 6). The refined atomic displacement parameters of apical and inner chlorines (Table 8 and Table S3) were comparable to those of the trigonal $Cs_2Mo_6Cl_{14}$ compound. Moreover, as in $Cs_2Mo_6Cl_{14}$ the shorter Mo-Cl

distances in the $[Mo_6Cl^i_8Cl^a_6]^{2-}$ unit are observed between Mo atoms and chlorine atoms in apical position (Table 5). Refinements performed at 293 K and 150 K lead to similar refined atomic coordinates (Table 8) indicating no structural modification at low temperature. However, measurement performed at 150 K on the same single-crystal leads to cell parameters *a* = 19.5004(11) Å, *b* = 15.1808(8) Å, *c* = 9.3527(5) Å, β = 115.698(3)°, V = 2494.8(2) Å^3 (Table 2). These results highlighted that both *b* and *c* parameters are larger at 150 K than those at room temperature (the volume of the unit cell being constant) which is in apparent contradiction with the thermal contraction expected when the temperature decreases and the lower isotropic (Table 8) and anisotropic (Table S3) displacement parameters refined at 150 K compared to those at 293 K due to thermal motion reduction. This behavior can be the consequence of a reorganization of the water molecules through stronger hydrogen bonds with chlorine atoms when the temperature decreases. The crystal structure of $Cs_2Mo_6Cl_{14}.H_2O$ consists of 4 $[Mo_6Cl_{14}]^{2-}$ units per unit cell centered on a *4c* (¼, ¼, 0) site of symmetry *-1*. This structure can be described from discrete $[Mo_6Cl^i_8Cl^a_6]^{2-}$ anionic cluster units arranged in a "A-A'-A-A'" pseudo close-packed prismatic stacking parallel to (*b*,*c*) plane [42] with both Cs^+ cations and water molecules located between the layers (Figure 7). Similar pseudo prismatic stacking was already observed in $CsErNb_6Br_{18}$ compound [45]. On the contrary to $CsErNb_6Br_{18}$ crystal structure, the three-fold axes of the clusters in $Cs_2Mo_6Cl_{14}.H_2O$ are not oriented perpendicularly to the pseudo prismatic planes but are tilted from the normal of the plane by about 11°.

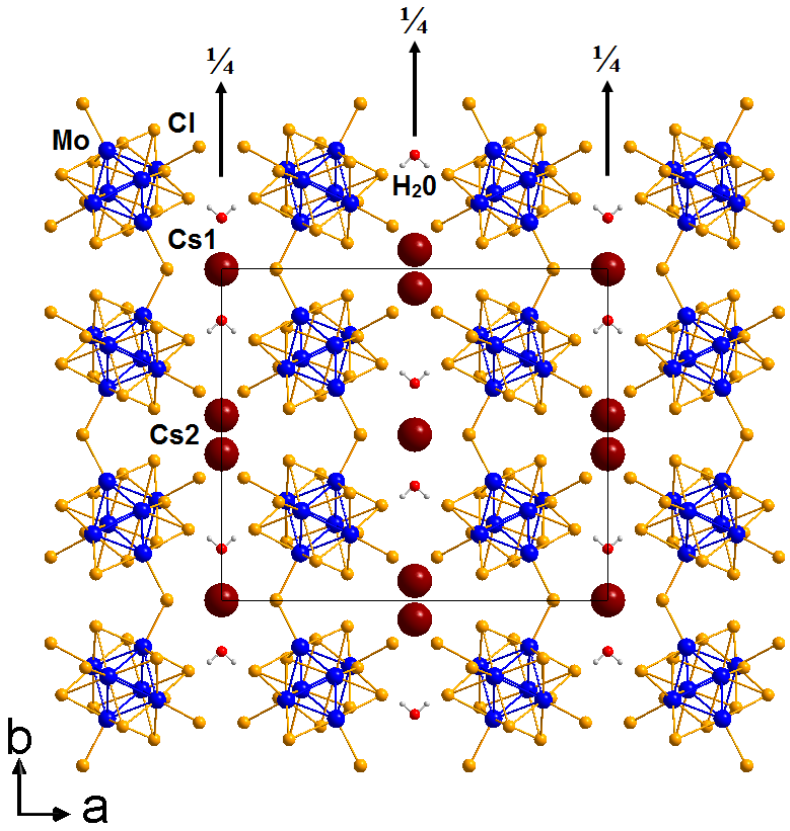


Figure 7: Crystal structure representation along the *c*-axis of $Cs_2Mo_6Cl_{14}.H_2O$

The crystal structure of $Cs_2Mo_6Cl_{14}.H_2O$ consists of four $[Mo_6Cl_{14}]^{2-}$ units per unit cell centered on the (¼, ¼, 0) inversion centers (Figure 6 and Figure 7), eight Cs^+ cations and four water molecules. Four Cs^+ cations occupy special positions of *-1* symmetry site (Cs1 atoms) on the (0, 0, 0) inversion centers *i* (according to Schoenflies notation) and the four remaining Cs^+ cations occupy special positions of *2* symmetry site (Cs2 atoms) on the two-fold axis C_2 (according to Schoenflies notation). Cs1 atoms are located in two distorted square-planes of four $[Mo_6Cl_{14}]^{2-}$ cluster units on one hand, and two Cs1 atoms and two H_2O molecules on the other hand, which are perpendicular one to the other (Figure 8). Cs2 atoms are located in a prismatic polyhedron of $[Mo_6Cl_{14}]^{2-}$ cluster units face-capped by two Cs2 atoms and one H_2O molecule (Figure 8). The $Cs_2[Mo_6Cl_{14}]$ framework is filled by four H_2O molecules located in a prismatic environment of $[Mo_6Cl_{14}]^{2-}$ cluster units face-capped by three Cs atoms (Figure 9). The oxygen atoms occupy special positions on the two-fold axes C_2 (according to Schoenflies notation) (Figure 7 and Figure 9). The hydrogen atoms occupy a general position and point to apical chlorines Cl5 of two different $[Mo_6Cl_{14}]^{2-}$ cluster units suggesting hydrogen bonds between these atoms (*i.e.* 2.70

Å and 2.68 Å at 293 K and 150 K, respectively). The two lone pairs of electrons of the oxygen atoms point to two Cs1 cations. Finally, the environment of H_2O molecules is completed by two apical chlorines Cl6, two inner chlorines Cl1 and one Cs2 atom (Figure 9) leading to a distorted octahedron of Cl atoms three-capped by Cs atoms.

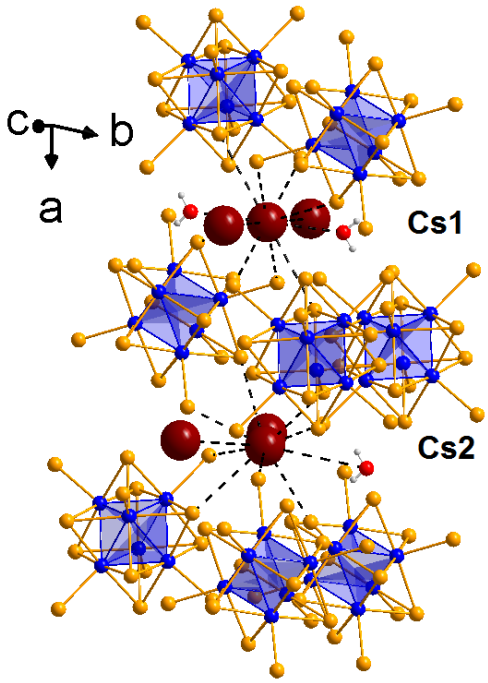


Figure 8: Representation of the cesium cation environments in $Cs_2Mo_6Cl_{14}.H_2O$. Chlorine atoms were omitted for clarity

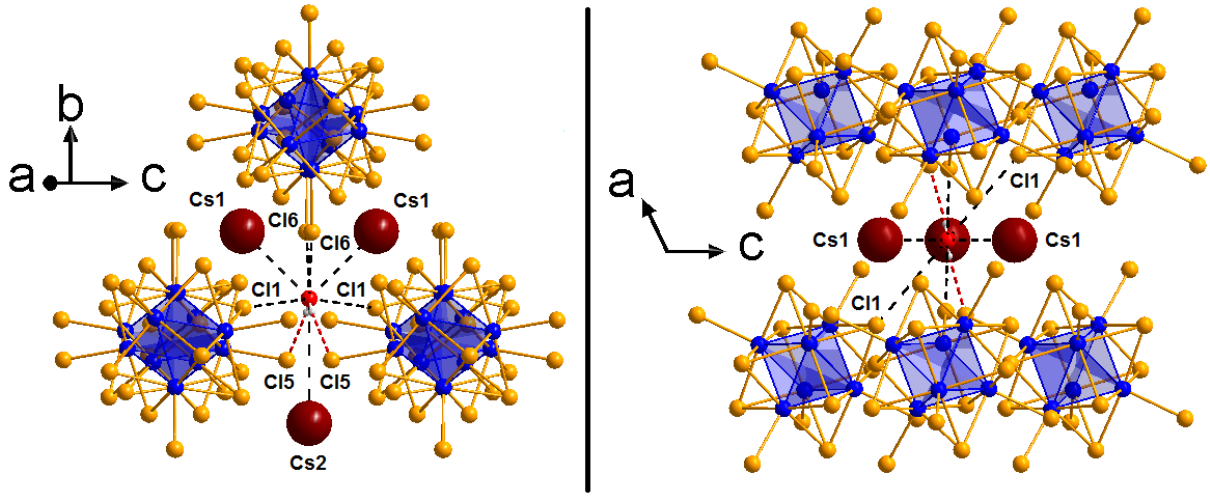


Figure 9: Representation of the water molecule environment in $Cs_2Mo_6Cl_{14}.H_2O$. Hydrogen bonds are represented in dotted red lines

As previously mentioned, water-filled $A_2Mo_6Cl_{14}.H_2O$ (A = NH_4, K, Rb) compounds were already reported in literature [29,44]. However, our crystal structure model differs from that reported by Nägele *et al.* [44] by the inversion of the water molecule and the counter cation (*i.e.* NH_4^+ or Cs^+) both centered on a *4e* site. The distinction between H_2O and NH_4 molecules using XRD is difficult and was able to lead in their refinement to ambiguous interpretation. Thus, Flemström *et al.* have studied the influence of such molecule inversion on the total energy of the system by theoretical calculations carried out with DFT method under generalized-gradient-approximation [29]. Their results indicate that the lower energy configuration is not that reported by Nägele *et al.* [44]. On contrary, distinction between H_2O molecule and Cs atom using XRD is easier. Thanks to heavier counter cations, $Cs_2Mo_6Cl_{14}.H_2O$ exhibits a chemical composition that enables to better determine

experimentally the exact positions of the counter-cations and water molecules in the monoclinic crystal structure than that of $(NH_4)_2Mo_6Cl_{14}.H_2O$. Moreover, our crystal structure refinement supports the theoretical results of Flemström *et al.* [29]. However, our model also differs from that reported by Flemström *et al.* [29], by the fact that they used a lower symmetry space group (*i.e. Ia* instead of *C*2/*c*), leading to slightly structural differences. It is worth noting that $Cs_2Mo_6Cl_{14}.H_2O$ is unstable over time and tends to transform to $Cs_2Mo_6Cl_{14}$ due to water evaporation, inducing crystal structure transformation from monoclinic to trigonal structure. This structural transition related to water evaporation can be reasonably extended to $A_2Mo_6Cl_{14}.H_2O$ (A = NH_4, K, Rb) compounds and thus could explain the slight crystal structure disorder observed by Flemström *et al.* on single-crystal of these compounds yielding them to refine the crystal structure in the non-centrosymmetric space group *Ia* [29]. Considering these results, the structure of $A_2Mo_6Cl_{14}.H_2O$ (A = NH_4, K, Rb, Cs) compounds could be regarded as a water-filled $Rb_2W_6Br_{14}$-type structure. However, a counter cation (*i.e.* Rb) disorder on several crystallographic sites is reported in $Rb_2W_6Br_{14}$ [42], which is not the case in $Cs_2Mo_6Cl_{14}.H_2O$. On the basis of this structural analysis, it can be concluded that $Cs_2Mo_6Cl_{14}.H_2O$ crystallizes in its own type structure.

3.4. X-ray powder diffraction

Pure powder samples of $Cs_2Mo_6X_{14}$ and $Cs_2Mo_6X_{14}.H_2O$ (with X = Cl and Br) have been obtained from evaporation of an acetone solution of the respective $Cs_2Mo_6X_{14}$ compounds and studied by XRPD. Refinements of the $Cs_2Mo_6X_{14}$ compounds have been performed with the centrosymmetric crystal structure (*P*-31*c* space group, Table 3), and those of the $Cs_2Mo_6X_{14}.H_2O$ compounds with the crystal structure determined on $Cs_2Mo_6Cl_{14}.H_2O$ single-crystal (Table 8). Cell parameters refined from room temperature XRPD data are gathered in Table 9. In agreement with the anionic radius of bromine (*i.e.* 1.82 Å) and chlorine (*i.e.* 1.67 Å), bromides evidence larger cell parameters than chlorides (Table 9), leading to a volume expansion at room temperature of 14.4% and 13.7% for $Cs_2Mo_6X_{14}$ and $Cs_2Mo_6X_{14}.H_2O$ compounds, respectively. The volume per formula unit V/Z is 592.0 $Å^3$, 624.9 $Å^3$, 677.1 $Å^3$, and 710.7 $Å^3$ in $Cs_2Mo_6Cl_{14}$, $Cs_2Mo_6Cl_{14}.H_2O$, $Cs_2Mo_6Br_{14}$, and $Cs_2Mo_6Br_{14}.H_2O$, respectively (Table 9). Considering that both $[Mo_6X_{14}]^{2-}$ cluster units (*i.e.* equivalent Mo-Mo, Mo-Cl^i, and Mo-Cl^a distances, Table 5) and Cs cations occupy the same volume in $Cs_2Mo_6X_{14}$ and $Cs_2Mo_6X_{14}.H_2O$ compounds, we can deduce that a water molecule inserted in $[Mo_6X_{14}]^{2-}$ cluster units framework occupy at room temperature a volume of 33(1) $Å^3$.

Table 9: Cell parameters at room temperature of $Cs_2Mo_6X_{14}$ and $Cs_2Mo_6X_{14}.H_2O$ (X = Cl, Br) compounds determined from Rietveld refinements of powder XRD data

	$Cs_2Mo_6Cl_{14}$	$Cs_2Mo_6Br_{14}$	$Cs_2Mo_6Cl_{14}.H_2O$	$Cs_2Mo_6Br_{14}.H_2O$
Space group	*P*-31*c*	*P*-31*c*	*C*2/*c*	*C*2/*c*
Z	2	2	4	4
a (Å)	9.810(1)	10.186(1)	19.578(1)	20.595(1)
b (Å)	9.810(1)	10.186(1)	15.151(1)	15.614(1)
c (Å)	14.206(1)	15.069(1)	9.347(1)	9.791(1)
β (°)	90	90	115.64(1)	115.45(1)
V ($Å^3$)	1184.0(1)	1354.1(1)	2499.7(1)	2842.8(2)
V/Z ($Å^3$)	592.0	677.1	624.9	710.7
R_{Bragg} ; R_f	17.5 ; 18.1	15.8 ; 29.7	17.6 ; 14.5	8.87 ; 6.00
R_{wp} ; R_{exp}	37.1 ; 28.73	14.9 ; 7.16	215.3 ; 8.16	9.91 ; 5.96
χ^2	1.66	4.33	3.54	2.77

4. Crystal structure relationship between $Cs_2Mo_6Cl_{14}$ and $Cs_2Mo_6Cl_{14}.H_2O$

As previously mentioned, the crystal structure of $Cs_2Mo_6Cl_{14}$ can be described from discrete $[Mo_6Cl^i_8Cl^a_6]^{2-}$ anionic cluster units arranged in a "A-B-A-B" close-packed hexagonal stacking along the *c*-axis, leading to two different intercluster Mo_6-Mo_6 distances (Figure 10 and Table 10): in the hexagonal planes (*i.e.* intra-layer) and between the hexagonal planes (*i.e.* inter-layer). The crystal structure of $Cs_2Mo_6Cl_{14}.H_2O$ can also be described from discrete $[Mo_6Cl^i_8Cl^a_6]^{2-}$ anionic cluster units arranged in a close-packed stacking parallel to (*b*,*c*) plane (Figure 10). However, in the layers the cluster units are arranged is a "A-A'-A-A'" pseudo prismatic configuration leading to two intercluster Mo_6-Mo_6 distances in the pseudo prismatic planes and one between the pseudo prismatic planes (Figure 10 and Table 10). In both structure, the inter-layer Mo_6-Mo_6 distances are shorter than the intra-layer Mo_6-Mo_6 distances though cesium atoms are located between the cluster layers.

Moreover, both intra- and inter-layer Mo_6-Mo_6 distances are shorter in the monoclinic structure compared to those of the trigonal structure (Table 10), indicating a more compact Mo_6 cluster framework in the first one. The thermal evolution of the intra- and inter-layer Mo_6-Mo_6 distances is related to the thermal evolution of the cell parameters. Indeed, in $Cs_2Mo_6Cl_{14}$ both intra- and inter-layer Mo_6-Mo_6 distances decrease with temperature (Table 10) in agreement with the reduction of the cell parameters (Table 1). In $Cs_2Mo_6Cl_{14}.H_2O$, the inter-layer Mo_6-Mo_6 distances (mainly dependent of the *a* parameter) decrease with temperature, while the intra-layer Mo_6-Mo_6 distances (only dependent of the *b* and *c* parameters) increase (Table 10). This anomalous thermal evolution is in agreement with the decrease of the *a* parameter and the increase of the *b* and *c* parameters when the temperature decreases (Table 2). It can be noted that an anomalous thermal evolution is also observed in $Cs_2Mo_6Cl_{14}.H_2O$ on the Mo-Mo distances, which are longer at 150K compared to 293K. Hence, the average Mo-Mo bond distance in $[Mo_6Cl^i_8Cl^a_6]^{2-}$ units of $Cs_2Mo_6Cl_{14}.H_2O$ is 2.605 Å at 293K and 2.620 Å at 150K (Table 5). Finally, considering only the Mo_6 cluster framework, the trigonal (*P*-31*c*) to monoclinic (*C*2/*c*) crystal structure transition can be described by a simple [1/3, 2/3, 0] translation of the hexagonal layers "B", the layers "A" keeping fixed. Such structural transition from hexagonal to prismatic stacking reduces the number of Mo_6-Mo_6 distances between the planes and induces a decrease of the inter-layer Mo_6-Mo_6 distances (Table 10).

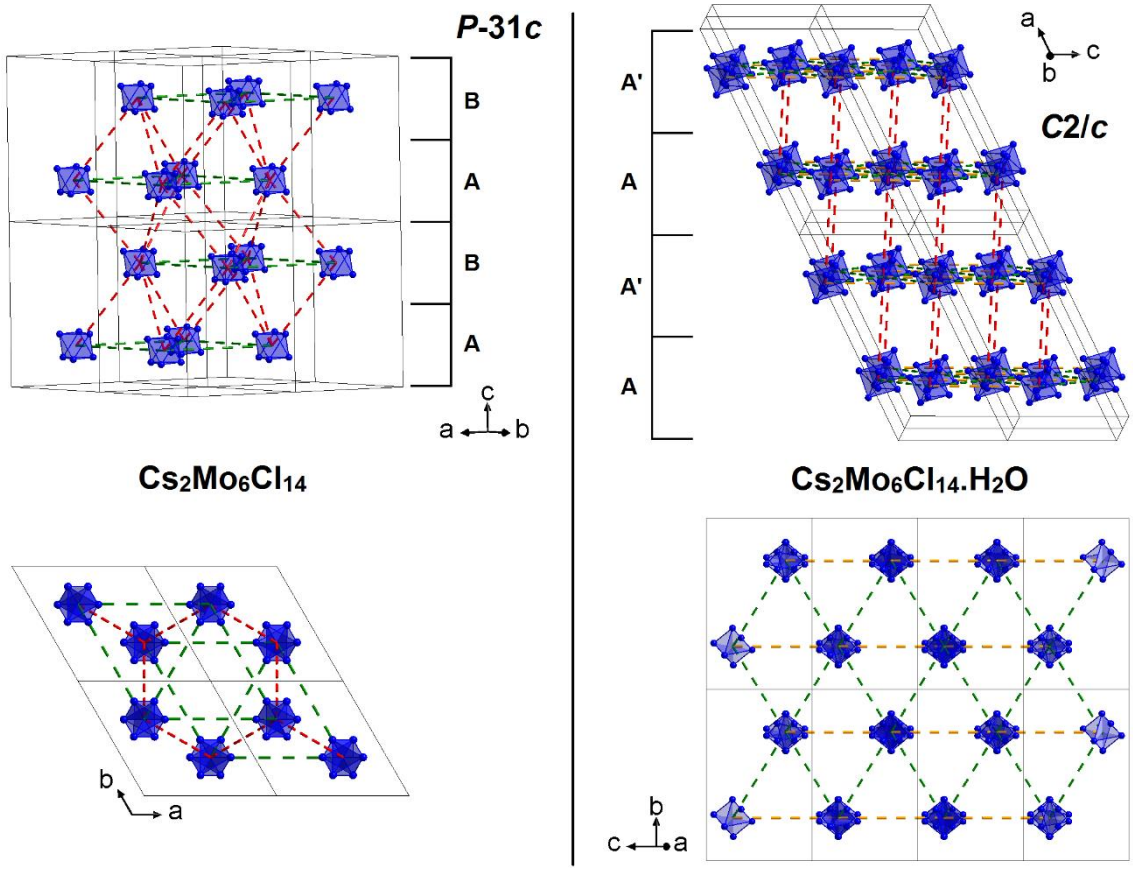


Figure 10: Representation of the intercluster Mo_6-Mo_6 distances in $Cs_2Mo_6Cl_{14}$ (left part) and $Cs_2Mo_6Cl_{14}.H_2O$ (right part). Cesium and chlorine atoms were omitted for clarity

Table 10: Main intercluster Mo_6-Mo_6 distances at room temperature and 150K in $Cs_2Mo_6Cl_{14}$ and $Cs_2Mo_6Cl_{14}.H_2O$ compounds determined from single crystal structure data

	$Cs_2Mo_6Cl_{14}$			$Cs_2Mo_6Cl_{14}.H_2O$		
Space group	*P*-31*c*	*P*-31*c*		*C*2/*c*	*C*2/*c*	
Temperature (K)	293(2)	150(2)		293(2)	150(2)	
Mo_6-Mo_6 (Å)			Δ^1			Δ^1
Inter-layer	9.086(1) ×6	9.028(1) ×6	-0.63	8.830(1) ×2	8.797(1) ×2	-0.37
Intra-layer	9.823(2) ×6	9.779(1) ×6	-0.45	8.895(1) ×4	8.915(1) ×4	+0.23
	-	-	-	9.340(1) ×2	9.353(1) ×2	+0.13

$^1\Delta$ = [Mo_6-Mo_6(150K) - Mo_6-Mo_6(293K)]/Mo_6-Mo_6(293K) (%)

5. Photophysical properties

Photoluminescence properties were studied on solid samples and the normalized emission spectra are shown in Figure 11. As expected, all the samples show very similar broadband emission at 762 nm for the chlorides and 796 nm for the bromides upon excitation with 410 nm. The new compounds $Cs_2Mo_6Cl_{14}.H_2O$ and $Cs_2Mo_6Br_{14}.H_2O$, bearing a water molecule present comparable emission profile as the parent compounds from which the phosphorescence properties have been known since the early 80s [15].

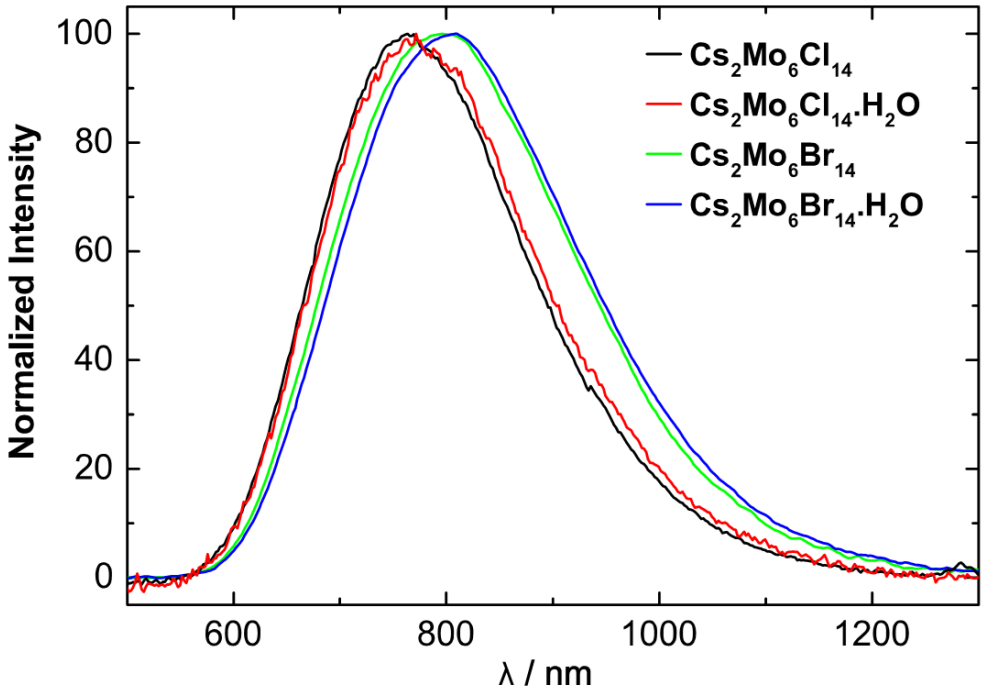


Figure 11: Emission spectra of $Cs_2Mo_6X_{14}$ and $Cs_2Mo_6X_{14}.H_2O$ (X = Cl, Br) under excitation at λ = 410 nm

6. Conclusions

We report here the synthesis, the crystal structures, and the comparative luminescent properties of the trigonal $Cs_2Mo_6X_{14}$ and monoclinic $Cs_2Mo_6X_{14}.H_2O$ (X = Cl, Br) cluster compounds. Trigonal and monoclinic structures are based on "A-B-A-B" hexagonal and "A-A'-A-A'" pseudo prismatic stacking mode of layers of $[Mo_6X^i_8X^a_6]^{2-}$ units, respectively. Cs^+ are located within the layers in triangular sites and between the layers in octahedral sites of $[Mo_6X^i_8X^a_6]^{2-}$ units in the trigonal structure, while in the monoclinic structure solvated $[Cs(H_2O)]^+$ are located only between the layers in distorted square-plan and prismatic sites of $[Mo_6X^i_8X^a_6]^{2-}$ units. Both $Cs_2Mo_6X_{14}$ (*P*-31*c*) and $Cs_2Mo_6X_{14}.H_2O$ (*C*2/*c*) powders are obtained from acetone solutions of Cs^+ and $[Mo_6X^i_8X^a_6]^{2-}$ units. The evaporation of the solvent using a rotavapor at room temperature and at 60°C favors the formation of $Cs_2Mo_6X_{14}.H_2O$ (*C*2/*c*) and $Cs_2Mo_6X_{14}$ (*P*-31*c*) powders, respectively. Moreover, powder of $Cs_2Mo_6X_{14}.H_2O$ (*C*2/*c*) transform irreversibly to $Cs_2Mo_6X_{14}$ (*P*-31*c*) on ambient atmosphere. Reversibly, dissolution of $Cs_2Mo_6X_{14}$ (*P*-31*c*) in acetone yields solutions of Cs^+ and $[Mo_6X^i_8X^a_6]^{2-}$ units from which $Cs_2Mo_6X_{14}$ (*P*-31*c*) and $Cs_2Mo_6X_{14}.H_2O$ (*C*2/*c*) powders can be obtained by control of evaporation. Single-crystals of $Cs_2Mo_6Cl_{14}$ and $Cs_2Mo_6Cl_{14}.H_2O$ were obtained by slow evaporation of a solution of acetonitrile with dichloromethane as antisolvent. The formation of $Cs_2Mo_6Cl_{14}.H_2O$ single-crystals is favored by addition of some drops of water. The ambiguous centric character of $Cs_2Mo_6Cl_{14}$ (*P*-31*c* vs *P*31*c*) already reported by Healy *et al.* [32] can be simply explained by the presence of $[Cs(H_2O)]^+$ among Cs^+ in freshly prepared samples. This centric character ambiguity cannot be elucidated by single-crystal X-ray investigations only, considering the fact that presence of $[Cs(H_2O)]^+$ among Cs^+ leads only to slight modifications of the unit cell parameters. Finally, comparison of photophysical properties of $Cs_2Mo_6Cl_{14}.H_2O$ and on the isotype $Cs_2Mo_6Br_{14}.H_2O$ with corresponding $Cs_2Mo_6X_{14}$ parent compounds, shows that the water molecule insertion and the $[Mo_6X^i_8X^a_6]^{2-}$ cluster units rearrangement from trigonal to monoclinic structure do not influence the emission profile.

Acknowledgements

The authors are indebted to the Institut Laue Langevin (Grenoble, France) for the provision of research facilities.

References

[1] S. Cordier, K. Kirakci, D. Méry, C. Perrin, D. Astruc, Inorg. Chim. Acta 359, 1705 (2006)

[2] F. Grasset, F. Dorson, S. Cordier, Y. Molard, C. Perrin, A.-M. Marie, T. Sasaki, H. Haneda, Y. Bando, M. Mortier, Adv. Mater. 20, 143 (2008)

[3] S. Cordier, F. Dorson, F. Grasset, Y. Molard, B. Fabre, H. Haneda, T. Sasaki, M. Mortier, S. Ababou-Girard, C. Perrin, J. Clust. Sci. 20, 9 (2009)

[4] Y. Molard, F. Dorson, V. Cîrcu, T. Roisnel, F. Artzner, S. Cordier, Angew. Chem. Int. Ed. 49, 3351 (2010)

[5] M.N. Sokolov, M.A. Mihailov, E.V. Peresypkina, K.A. Brylev, N. Kitamura, V.P. Fedin, Dalton Trans. 40, 6375 (2011)

[6] Y. Molard, C. Labbé, J. Cardin, S. Cordier, Adv. Funct. Mater. 23, 4821 (2013)

[7] M. Amela-Cortes, A. Garreau, S. Cordier, E. Faulques, J.-L. Duvail, Y. Molard, J. Mater. Chem. C 2, 1545 (2014)

[8] P. Kumar, S. Kumar, S. Cordier, S. Paofai, R. Boukherroub, S.L. Jain, RSC Adv. 4, 10420 (2014)

[9] S. Cordier, F. Grasset, Y. Molard, M. Amela-Cortes, R. Boukherroub, S. Ravaine, M. Mortier, N. Ohashi, N. Saito, H. Haneda, J. Inorg. Organomet. Polym. 25, 189 (2015)

[10] C. Godet, S. Ababou-Girard, B. Fabre, Y. Molard, A.B. Fadjie-Djomkam, S. Députier, M. Guilloux-Viry, S. Cordier, Diamond Relat. Mater. 55, 131 (2015)

[11] M. Amela-Cortes, S. Paofai, S. Cordier, H. Folliot, Y. Molard, Chem. Commun. 51 (2015) 8177-8180.

[12] Y. Zhao, R.R. Lunt, Adv. Energy Mater. 3, 1143 (2013)

[13] P.S. Kuttipillai, Y. Zhao, C.J. Traverse, R.J. Staples, B.G. Levine, R.R. Lunt, Adv. Mater. 28, 320 (2016)

[14] M. Potel, C. Perrin, A. Perrin, M. Sergent, Mat. Res. Bull. 21, 1239 (1986)

[15] A.W. Maverick, H.B. Gray, J. Am. Chem. Soc. 103, 1298 (1981)

[16] H.B. Gray, A.W. Maverick, Science 214, 1201 (1981)

[17] A. Barras, S. Cordier, R. Boukherroub, Appl. Catal. B 123-124, 1 (2012)

[18] A. Barras, M.R. Das, R.R. Devarapalli, M.V. Shelke, S. Cordier, S. Szunerits, R. Boukherroub, Appl. Catal. B 130-131, 270 (2013)

[19] M. Prévôt, M. Amela-Cortes, S.K. Manna, R. Lefort, S. Cordier, H. Folliot, L. Dupont, Y. Molard, Adv. Funct. Mater. 25, 4966 (2015)

[20] M. Amela-Cortes, Y. Molard, S. Paofai, A. Desert, J.-L. Duvail, N.G. Naumov, S. Cordier, Dalton Trans. 45, 237 (2016)

[21] S.K. Nayak, M. Amela-Cortes, C. Roiland, S. Cordier, Y. Molard, Chem. Commun. 51, 3774 (2015)

[22] S.K. Nayak, M. Amela-Cortes, M.M. Neidhardt, S. Beardsworth, J. Kirres, M. Mansueto, S. Cordier, S. Laschat, Y. Molard, Chem. Commun. 52, 3127 (2016)

[23] F. Grasset, F. Dorson, Y. Molard, S. Cordier, V. Demange, C. Perrin, V. Marchi-Artzner, H. Haneda, Chem. Commun. 39, 4729 (2008)

[24] T. Aubert, F. Grasset, S. Mornet, E. Duguet, O. Cador, S. Cordier, Y. Molard, V. Demange, M. Mortier, H. Haneda, J. Colloid Interface Sci. 341, 201 (2010)

[25] T. Aubert, F. Cabello-Hurtado, M.-A. Esnault, C. Neaime, D. Lebret-Chauvel, S. Jeanne, P. Pellen, C. Roiland, L. Le Polles, N. Saito, K. Kimoto, H. Haneda, N. Ohashi, F. Grasset, S. Cordier, J. Phys. Chem. C 117, 20154 (2013)

[26] N. Nerambourg, T. Aubert, C. Neaime, S. Cordier, M. Mortier, G. Patriarche, F. Grasset, J. Colloid Interface Sci. 424, 132 (2014)

[27] K. Kirakci, S. Cordier, C. Perrin, Z. Anorg. Allg. Chem. 631, 411 (2005)

[28] F.A. Cotton, R.M. Wing, R.A. Zimmerman, Inorg. Chem. 6, 11 (1967)

[29] A. Flemström, T.K. Hirsch, L. Eriksson, S. Lidin, Solid State Sci. 6, 509 (2004)

[30] F.W. Koknat, T.J. Adaway, S.I. Erzerum, S. Syed, Inorg. Nucl. Chem. Letters 16, 307 (1980)

[31] N. Saito, Y. Wada, P. Lemoine, S. Cordier, F. Grasset, T. Ohsawa, N. Saito, J.S. Cross, N. Ohashi, Jpn. J. Appl. Phys. 55, 075502 (2016)

[32] P.C. Healy, D.L. Kepert, D. Taylor, A.H. White, J. Chem. Soc. Dalton, 646 (1973)

[33] A. Altomare, M.C. Burla, M. Camalli, G. Cascarano, C. Giacovazzo, A. Guagliardi, A.G.G. Moliterni, G. Polidori, R. Spagna, J. Appl. Cryst. 32, 115 (1999)

[34] G.M. Sheldrick, Acta Cryst. C 71, 3 (2015)

[35] L.J. Farrugia, J. Appl. Cryst. 45, 849 (2012)

[36] J. Rodriguez-Carvajal, Physica B 192, 55 (1993)

[37] T. Roisnel, J. Rodriguez-Carvajal, Mater. Sci. Forum 378-381, 118 (2001)

[38] Y. Le Page, J. Appl. Cryst. 20, 264 (1987)

[39] Y. Le Page, J. Appl. Cryst. 21, 983 (1988)

[40] R.E. Marsh, Acta Cryst. B51, 897 (1995)

[41] V.F. Sears, Neutron News, 3, 26 (1992)

[42] Y.Q. Zheng, K. Peters, Y. Grin, H.G. von Schnering, Z. Anorg. Allg. Chem. 624, 506 (1998)

[43] K. Kirakci, S. Cordier, O. Hernandez, T. Roisnel, F. Paul, C. Perrin, J. Solid State Chem. 178, 3117 (2005)

[44] A. Nägele, K. Gibson, A. Lachgar, H.J. Meyer, Z. Anorg. Allg. Chem. 625, 799 (1999)

[45] S. Cordier, C. Perrin, M. Sergent, Z. Anorg. Allg. Chem. 619, 621 (1993)

Supplementary data

Table S1: Anisotropic displacement parameters of $Cs_2Mo_6Cl_{14}$ refined at room temperature

P-31*c*						
Atom	U_{11}	U_{22}	U_{33}	U_{23}	U_{13}	U_{12}
Cs1	0.0307(10)	0.0307(10)	0.077(6)	0	0	0.0153(5)
Cs2	0.0296(8)	0.0296(8)	0.096(3)	0	0	0.0148(4)
Mo1	0.0121(5)	0.0139(5)	0.0170(4)	0.0005(4)	-0.0011(4)	0.0074(4)
Cl1	0.0249(15)	0.0249(15)	0.013(2)	0	0	0.0125(8)
Cl2	0.0189(14)	0.0163(14)	0.0275(15)	-0.0039(11)	-0.0036(11)	0.0020(11)
Cl3	0.0204(17)	0.042(2)	0.0360(17)	0.0044(17)	-0.0132(13)	0.0148(17)

*P*31*c*						
Atom	U_{11}	U_{22}	U_{33}	U_{23}	U_{13}	U_{12}
Cs1	0.0299(6)	0.0299(6)	0.090(2)	0	0	0.0150(3)
Cs2	0.0310(6)	0.0310(6)	0.0908(17)	0	0	0.0155(3)
Mo1a	0.0111(7)	0.0127(8)	0.0164(7)	0.0011(5)	-0.0017(6)	0.0064(6)
Mo1b	0.0121(7)	0.0128(7)	0.0166(7)	0.0009(6)	0.0008(6)	0.0059(6)
Cl1a	0.021(3)	0.021(3)	0.017(5)	0	0	0.0104(14)
Cl1b	0.028(3)	0.028(3)	0.011(4)	0	0	0.0140(15)
Cl2a	0.016(2)	0.015(2)	0.024(2)	-0.0052(17)	-0.0069(17)	0.003(2)
Cl2b	0.015(2)	0.022(2)	0.027(2)	0.0003(16)	0.0026(17)	0.0097(17)
Cl3a	0.022(2)	0.032(3)	0.037(2)	0.0030(18)	-0.011(2)	0.0159(19)
Cl3b	0.045(3)	0.029(3)	0.035(2)	-0.011(2)	0.002(2)	0.021(2)

$$T_j = exp(-2\pi^2[U_{11}h^2a^{*2} + U_{22}k^2b^{*2} + U_{33}l^2c^{*2} + 2U_{23}klb^*c^* + 2U_{13}hla^*c^* + 2U_{12}hka^*b^*])$$

Table S2: Anisotropic displacement parameters of $Cs_2Mo_6Cl_{14}$ refined at 150 K

P-31*c*						
Atom	U_{11}	U_{22}	U_{33}	U_{23}	U_{13}	U_{12}
Cs1	0.0169(12)	0.0169(12)	0.060(4)	0	0	0.0084(6)
Cs2	0.0161(9)	0.0161(9)	0.052(2)	0	0	0.0080(5)
Mo1	0.0071(7)	0.0089(6)	0.0105(6)	-0.0015(6)	-0.0018(5)	0.0051(6)
Cl1	0.0127(18)	0.0127(18)	0.010(3)	0	0	0.0063(9)
Cl2	0.0122(19)	0.0106(18)	0.0158(18)	0.0004(15)	-0.0027(15)	-0.0011(15)
Cl3	0.0072(19)	0.035(3)	0.0205(19)	0.000(2)	-0.0059(16)	0.0095(19)

*P*31*c*						
Atom	U_{11}	U_{22}	U_{33}	U_{23}	U_{13}	U_{12}
Cs1	0.0164(4)	0.0164(4)	0.0549(11)	0	0	0.0082(2)
Cs2	0.0178(4)	0.0178(4)	0.0493(10)	0	0	0.0089(2)
Mo1a	0.0066(5)	0.0076(5)	0.0107(6)	0.0003(4)	-0.0009(4)	0.0038(4)
Mo1b	0.0067(5)	0.0068(5)	0.0093(6)	0.0007(4)	0.0009(4)	0.0031(4)
Cl1a	0.0107(17)	0.0107(17)	0.013(3)	0	0	0.0054(8)
Cl1b	0.0134(17)	0.0134(17)	0.007(3)	0	0	0.0067(9)
Cl2a	0.084(13)	0.0100(14)	0.0152(17)	-0.0009(13)	-0.0035(12)	0.0024(13)
Cl2b	0.0098(14)	0.0156(16)	0.0121(15)	0.0007(11)	0.0020(12)	0.0078(12)
Cl3a	0.0129(15)	0.0193(16)	0.0197(17)	0.0034(13)	-0.0060(13)	0.0093(13)
Cl3b	0.027(2)	0.0156(16)	0.0191(18)	-0.0049(14)	-0.0011(13)	0.0136(15)

$$T_j = exp(-2\pi^2[U_{11}h^2a^{*2} + U_{22}k^2b^{*2} + U_{33}l^2c^{*2} + 2U_{23}klb^*c^* + 2U_{13}hla^*c^* + 2U_{12}hka^*b^*])$$

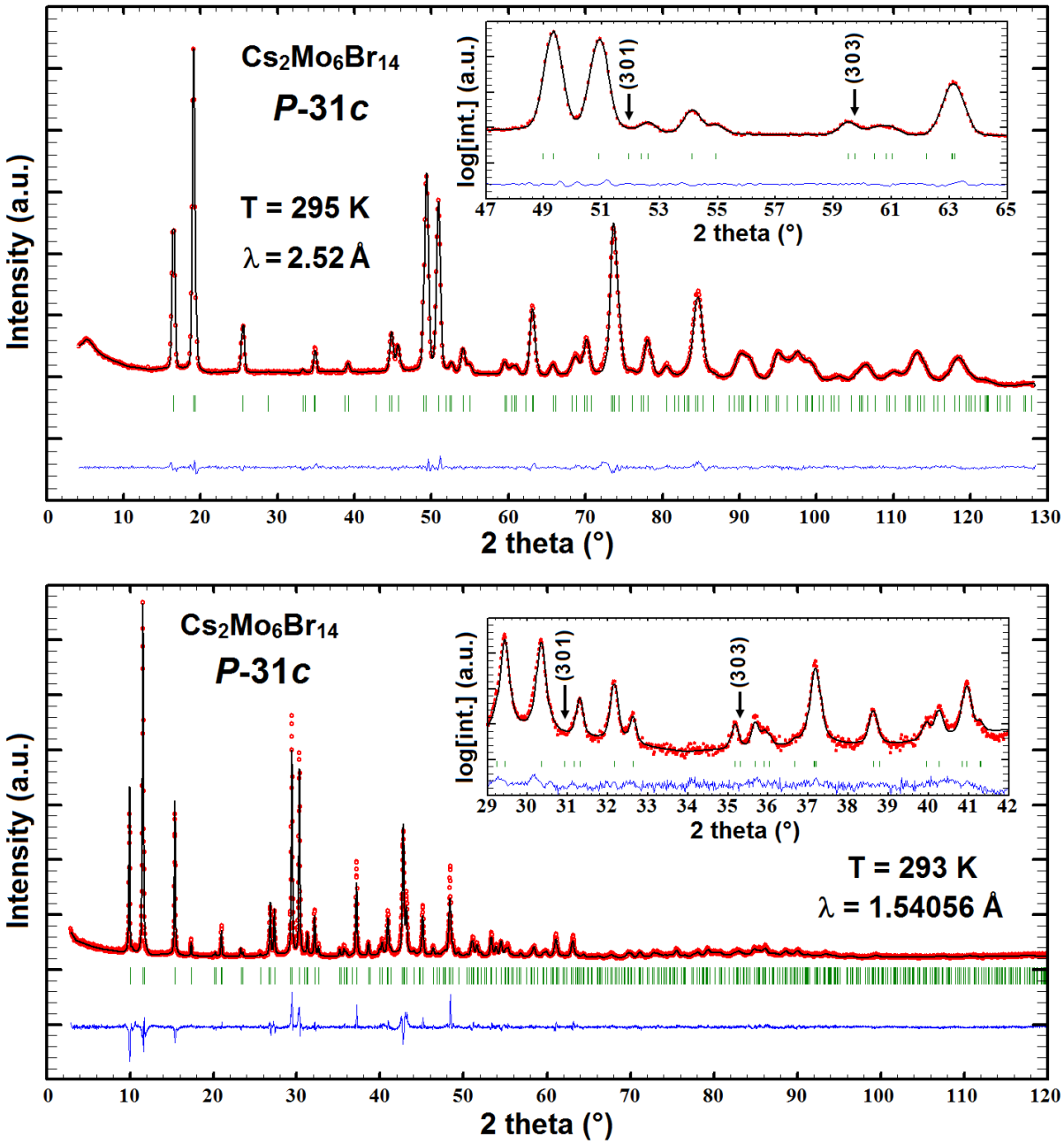


Figure S1: Combined neutron (top pattern) and X-ray (bottom pattern) powder diffraction refinement of $Cs_2Mo_6Br_{14}$ at room temperature with centrosymmetric space group *P*-31*c*

Table S3: Anisotropic displacement parameters refined at room temperature and 150 K for $Cs_2Mo_6Cl_{14}.H_2O$

T = 293 K						
Atom	U_{11}	U_{22}	U_{33}	U_{23}	U_{13}	U_{12}
Cs1	0.0367(2)	0.0883(3)	0.0398(2)	0.0050(2)	0.0209(2)	-0.0030(2)
Cs2	0.0441(2)	0.0324(2)	0.0265(2)	0	0.0132(2)	0
Mo1	0.0188(2)	0.0217(2)	0.0185(2)	0.0016(1)	0.0098(1)	0.0014(1)
Mo2	0.0185(2)	0.0182(2)	0.0205(2)	0.0010(1)	0.0087(1)	-0.0005(1)
Mo3	0.0175(2)	0.0204(2)	0.0176(2)	0.0029(1)	0.0067(1)	0.0020(1)
Cl1	0.0276(4)	0.0303(3)	0.0199(3)	-0.0031(3)	0.0084(3)	-0.0017(3)
Cl2	0.0260(4)	0.0228(3)	0.0295(3)	0.0002(3)	0.0126(3)	0.0047(3)
Cl3	0.0187(3)	0.0294(3)	0.0301(4)	0.0026(3)	0.0111(3)	0.0001(2)
Cl4	0.0295(4)	0.0273(3)	0.0262(3)	0.0086(3)	0.0147(3)	0.0011(3)
Cl5	0.0403(5)	0.0523(5)	0.0354(4)	0.0015(4)	0.0267(4)	0.0072(4)
Cl6	0.0344(4)	0.0246(3)	0.0447(5)	-0.0057(3)	0.0211(4)	-0.0077(4)
Cl7	0.0295(4)	0.0422(4)	0.0260(4)	0.0094(3)	0.0059(3)	0.0105(3)
O1	0.041(3)	0.050(3)	0.168(7)	0	0.030(4)	0

T = 150 K						
Atom	U_{11}	U_{22}	U_{33}	U_{23}	U_{13}	U_{12}
Cs1	0.0174(1)	0.0361(2)	0.0190(1)	0.0007(1)	0.0102(1)	-0.0018(1)
Cs2	0.0219(1)	0.0153(1)	0.0129(1)	0	0.0067(1)	0
Mo1	0.0090(1)	0.0103(1)	0.0093(1)	0.0007(1)	0.0048(1)	0.0006(1)
Mo2	0.0089(1)	0.0087(1)	0.0102(1)	0.0003(1)	0.0044(1)	-0.0003(1)
Mo3	0.0082(1)	0.0098(1)	0.0088(1)	0.0013(1)	0.0033(1)	0.0008(1)
Cl1	0.0136(2)	0.0149(2)	0.0099(2)	-0.0013(2)	0.0043(2)	-0.0009(2)
Cl2	0.0128(2)	0.0110(2)	0.0151(2)	0.0001(2)	0.0065(2)	0.0022(2)
Cl3	0.0089(2)	0.0139(2)	0.0150(2)	0.0010(2)	0.0051(2)	0.0000(2)
Cl4	0.0141(2)	0.0131(2)	0.0132(2)	0.0039(2)	0.0070(2)	0.0005(2)
Cl5	0.0195(2)	0.0242(3)	0.0174(2)	0.0008(2)	0.0130(2)	0.0031(2)
Cl6	0.0164(2)	0.0118(2)	0.0213(2)	-0.0023(2)	0.0099(2)	-0.0030(2)
Cl7	0.0137(2)	0.0203(2)	0.0131(2)	0.0042(2)	0.0032(2)	0.0045(2)
O1	0.020(2)	0.024(2)	0.070(2)	0	0.013(2)	0

$$T_j = exp(-2\pi^2[U_{11}h^2a^{*2} + U_{22}k^2b^{*2} + U_{33}l^2c^{*2} + 2U_{23}klb^*c^* + 2U_{13}hla^*c^* + 2U_{12}hka^*b^*])$$